Title

Interaction of a normally-incident plane wave with a nonlinear poroelastic fracture

Journal
The Journal of the Acoustical Society of America, 146(3)

ISSN
0001-4966

Authors
Nakagawa, Seiji
Pride, Steven R
Nihei, Kurt T

Publication Date
2019-09-01

DOI
10.1121/1.5124691

Peer reviewed

Interaction of a normally-incident plane wave with a nonlinear poroelastic fracture

Seiji Nakagawa,[a] Steven R. Pride, and Kurt T. Nihei

Energy Geosciences Division, Earth & Environmental Sciences Area (EESA), Lawrence Berkeley National Laboratory, Berkeley, California 94720, USA

[a]Electronic mail: snakagawa@lbl.gov

ABSTRACT

While it has been recognized that a large amplitude incident wave upon a dry fracture can exhibit nonlinear seismic wave scattering due to its stress-dependent mechanical compliance, the impact of pore fluid in the fracture and a fluid-filled poroelastic background medium—features common for fractures in the Earth—are not well understood. As a first step toward an understanding of the nonlinear poroelastic response of elastic waves in fractured media, analytical approximate formulas are used for the amplitude and phase of a normally incident plane wave using a perturbation method, assuming a fluid-filled, highly compliant nonlinear interface embedded in a linear poroelastic solid. The stress-closure behavior of the fracture is modeled by nonlinear, poroelastic displacement-discontinuity boundary conditions (a linear–slip interface). The theory predicts that the static ("Direct current," or DC) and higher-order-harmonic waves produced by the nonlinear scattering can be greatly reduced by the presence of fluid in the fracture. This, however, depends upon a number of parameters, including fracture compliance, fluid properties (compressibility and viscosity), and the permeability of the background medium, as well as environmental parameters such as the initial fluid pressure and stress acting on the fracture. The static effect produces low-frequency fluid pressure pulses when a finite-duration wave is incident upon the fracture—behavior unique to fluid-filled fractures within a poroelastic medium.

I. INTRODUCTION

Imperfect interfaces in elastic solids, such as fractures and cracks, are known to exhibit strongly nonlinear stress-deformation behavior. In nondestructive testing, nonlinear elastic wave scattering from imperfect interfaces larger than expected from the nonlinearity in the bulk material properties alone has been recognized, typically through the generation of second- and higher-order harmonics (Buck *et al.*, 1978; Richardson, 1979). This type of nonlinearity—contact acoustic nonlinearity (CAN)—is caused by the changes in the local contact stiffness by wave-induced stresses, and has been studied and used for nondestructive detection of imperfect bonds and for characterization of local contact properties (Donskoy *et al.*, 2001; Hirsekorn, 2001; Van Den Abeele *et al.*, 2000).

Nonlinear scattering of seismic waves by a thin, flat, partially contacting ("imperfect" or "partially welded") interface can be examined using a modified form of the linear–slip interface model, which is frequently used for linear scattering of waves (e.g., Baik and Thompson, 1984; Schoenberg, 1980). This involves power-series expansion of the interface's nonlinear stress-closure relationship that expresses how displacement discontinuities across the interface depend on the stress that is continuous across the interface. Subsequent use of a perturbation method to expand the wave-induced displacement-discontinuity versus stress relation into a perturbation series allows the nonlinearity to be analytically addressed. For each order of the perturbation expansion, linear boundary conditions at the interface are derived, and the scattered waves are determined for a given incident wave. Pecorari (2003) solves nonlinear plane wave scattering off an interface characterized by the micromechanical contact model developed by Greenwood and Williamson (1996). This model involves nonlinear changes in both normal and shear contact stiffnesses as well as frictional slip between sheared asperities. Kim *et al.* (2006) examine plane wave scattering from an elastic-plastic contact and compare the theoretical predictions against laboratory measurements. Biwa *et al.* (2004) conduct a similar analysis as Pecorari, using several types of nonlinear contact stress-displacement relationships.

In contrast to the imperfect interfaces involved in nondestructive testing of engineered parts, compliant fractures in rock within the Earth's subsurface are often filled with fluids and are subject to high normal stress prior to wave arrival. This suppresses the nonlinear behavior of the fractures, resulting in reduced amplitudes of nonlinearly generated harmonics. However, when the effective stress acting on a fracture is reduced as a result of increasing pore pressure (e.g., induced by fluid injection) or by reducing confining stress (e.g., excavation-induced stress relief or stress changes following an earthquake), the stress-deformation relationship can become more highly nonlinear again. In this case, large-amplitude seismic waves propagating through the rock-fracture system can exhibit nonlinear behavior, which may prove useful for subsurface fracture detection and stress evaluation when combined with estimation or measurements of the pore pressure. A new theory needs to be developed for predicting the magnitude of the nonlinear scattering in poroelastic media and determining the sensitivity to material properties such as the rock matrix and pore fluid stiffnesses, permeability of the rock matrix, nonlinear stress-closure relationships of the fracture, and environmental parameters such as stress, pore pressure, and wave frequency. Additionally, processes unique to a fracture embedded within a porous, permeable rock, such as nonlinear relaxation of wave-induced fluid pressure in the fracture into the host rock, need to be investigated.

In this paper, we examine the nonlinear seismic response of a compliant, fluid-filled fracture embedded within a linear poroelastic host material. After a brief review of the theory of dynamic linear poroelasticity in Sec. II A, in Sec. II B, we review the earlier poroelastic linear-slip fracture discontinuity conditions derived by Nakagawa and Schoenberg (2007) in which the fracture compliances are taken to be independent of the wave-induced stressing. This serves as a basis for the nonlinear poroelastic fracture boundary conditions of Secs. II C and II D in which the fracture opening and closing caused by an incident wave and the fluid displacements from the wave-stressed fracture into the poroelastic host are allowed to be nonlinearly dependent on the wave stresses. However, in the present model, the nonlinearity attributed to hysteretic responses induced by friction and fluid-mediated slow changes of solid–solid interfaces (e.g., Johnson and Jia, 2005; Van Den Abeele *et al.*, 2002) and are not considered either for the fracture or the host medium.

Given such nonlinear fracture displacement-discontinuity boundary conditions, a perturbation expansion is then used in Secs. II E and II F to derive analytical expressions for the reflection and transmission of plane waves from the fracture. Throughout, we limit our analysis to the case of a compressional wave normally incident upon a fracture, thus excluding the coupling between *P* and *S* waves and nonlinear scattering due to shearing of the fracture. Finally, in Sec. III, the magnitude of the resulting nonlinear harmonics in the scattered waves is examined numerically for an example set of poroelastic rock matrix, fracture and fluid properties. Time-domain waveforms are also computed for a narrow-band incident pulse.

II. THEORY

In this theory section, after a quick review of poroelastic uniaxial response that will be needed throughout the paper, we derive a set of boundary conditions for nonlinear, plane poroelastic wave scattering by a fluid-filled compliant fracture embedded in an isotropic linear poroelastic background host. We then use a perturbation expansion to model how a normally incident plane compressional wave scatters from the fracture into nonlinear transmitted and reflected fast and slow compressional waves.

A. Poroelastic uniaxial response

The laws of isotropic poroelastic response are well established, e.g., Biot (1962), Burridge and Keller (1981), and Pride *et al.* (1992) all provide different derivations that yield the same results. In the frequency domain with $e^{-i\omega t}$ time dependence, the poroelastic laws are given by the two force balances

$$\nabla \cdot \boldsymbol{\tau} = -\omega^2(\rho\ \boldsymbol{u} + \rho_f\ \boldsymbol{w}), (1)$$

$$-\nabla p_f = -\omega^2(\rho_f\ \boldsymbol{u} + \widetilde{\rho}\ \boldsymbol{w}), (2)$$

the first being on the total bulk material and the second on the fluid in relative motion to the solid, and by the constitutive laws

$$d\boldsymbol{\tau} + dP_c\boldsymbol{I} = G\left(\nabla d\boldsymbol{u} + (\nabla d\boldsymbol{u})^T - \frac{2}{3}(\nabla \cdot d\boldsymbol{u})\boldsymbol{I}\right), (3)$$

$$-dP_c = K_U \ \nabla \cdot d\boldsymbol{u} + C \ \nabla \cdot d\boldsymbol{w}, (4)$$

$$-dp_f = C \ \nabla \cdot d\boldsymbol{u} + M \ \nabla \cdot d\boldsymbol{w}. (5)$$

The various response fields are the total stress tensor $\boldsymbol{\tau}$ acting on the porous material, the associated confining pressure $P_c = -(\tau_{11} + \tau_{22} + \tau_{33})/3$, the fluid pressure p_f, the solid displacements $\boldsymbol{u}$, and the displacement of fluid relative to the solid $\boldsymbol{w}$. The "*d*" in front of the response fields in the constitutive laws of Eqs. (3)–(5) corresponds to a small differential increment from a reference state, i.e., these constitutive laws are derived by taking derivatives of a poroelastic strain-energy function. In the time domain, further dividing through by dt would give a velocity and stress-rate formulation of the poroelastic constitutive laws with $\boldsymbol{v} = d\boldsymbol{u}/dt$ and $\boldsymbol{q} = d\boldsymbol{w}/dt$ being the solid velocity and the Darcy filtration velocity, respectively, and $d\boldsymbol{\tau}/dt = \partial\boldsymbol{\tau}/\partial t + \boldsymbol{v} \cdot \nabla\boldsymbol{\tau}$ and $dp_f/dt = \partial p_f/\partial t + (\boldsymbol{q}/\phi) \cdot \nabla p_f$ being the total derivative of stress and fluid pressure (where ϕ is porosity). We will not take a velocity and stress-rate formulation in what follows, however.

The various material properties are the undrained bulk modulus K_U, the Biot coupling modulus C, the fluid-storage modulus M, the bulk density of the porous material ρ, and the fluid density ρ_f. The effective viscous resistance to relative fluid motion $\tilde{\rho}$ written as an inertial property is defined as the complex parameter

$$\tilde{\rho}(\omega) = \frac{i\mu_f}{\omega k(\omega)}, (6)$$

where μ_f is the fluid viscosity and $k(\omega)$ is the so-called "dynamic permeability" (Johnson *et al.*, 1987). Lastly, G is the shear modulus of the material that is taken to be that of the framework of grains and independent of the fluid properties. If the elastic constants are not changing during a poroelastic problem, which corresponds to linear poroelasticity, Eqs. (3)–(5) can be integrated trivially with the effect of removing the d in front of the response fields. Otherwise, if the poroelastic moduli are changing, which corresponds to nonlinear poroelasticity, we need to take either a velocity and stress-rate formulation of the problem or be able to integrate the constitutive laws while allowing for the stress dependence of the elastic moduli.

Our focus in this paper is on the longitudinal (or uniaxial) plane wave response that we take to be in the x_3 direction. In this case, there are no lateral displacements so that $\partial du_1/\partial x_1 = \partial du_2/\partial x_2 = 0$, which results in $d\tau_{11} = d\tau_{22} = -dP_c - (2G/3)\partial du_3/\partial x_3$ and $d\tau_{33} = -P_c + (4G/3)\partial du_3/\partial x_3$. We now rewrite Eqs. (4) and (5) as uniaxial compressibility laws

$$\frac{\partial du_3}{\partial x_3} = \frac{1}{H_D} d\tau_{33} + \frac{\alpha}{H_D} dp_f, (7)$$

$$\frac{\partial dw_3}{\partial x_3} = -\frac{\alpha}{H_D} d\tau_{33} - \left(\frac{1}{M} + \frac{\alpha^2}{H_D} \right) dp_f, (8)$$

where the Biot-Willis constant α is the proportionality $C = \alpha M$ and the drained longitudinal modulus H_D is defined as $H_D = K_D + 4G/3$. The relation between the undrained bulk modulus and drained modulus is worked out to be $K_U = K_D + \alpha^2 M$. Similarly, the undrained longitudinal modulus is defined as $H_U = K_U + 4G/3$, and $H_U = H_D + \alpha^2 M$.

In order to determine how the fluid bulk modulus K_f is influencing these moduli, we assume that our porous medium is a Gassmann material, which means the framework of grains is composed of a single isotropic mineral having bulk modulus K_s. In this case, we have the Gassmann-material results that

$$\frac{1}{M} = \frac{\phi}{K_f} + \frac{\alpha - \phi}{K_s}, (9)$$

$$\alpha = 1 - \frac{K_D}{K_s}, (10)$$

where ϕ is again the porosity. Another Gassmann-material result is that the porosity changes as (Pride, 2005)

$$d\phi = -\left[\frac{(1-\phi)}{K_D} - \frac{1}{K_s}\right](dP_c - dp_f), (11)$$

which, for uniaxial response, results in

$$d\phi = \frac{(\alpha-\phi)}{H_D}\left\{d\tau_{33} + \left[1 + \frac{(1-\alpha)}{K_D}\frac{4G}{3}\right]dp_f\right\}. (12)$$

We will use this expression in Sec. II D 2.

Finally, for a plane displacement wave of amplitude U propagating in the $\pm x_3$ direction through a uniform porous material, we have that

$$u_3 = \pm U e^{i\omega[\pm s(\omega)x_3 - t]}, (13)$$

where $s(\omega)$ is the longitudinal complex slowness given as (cf. Pride, 2005)

$$2s^2 = \xi \mp \sqrt{\xi^2 - \frac{4(\rho\widetilde{\rho} - \rho_f^2)}{MH_D}}, (14)$$

with the parameter ξ defined as

$$\xi = \frac{\rho}{H_D} + \widetilde{\rho}\left(\frac{1}{M} + \frac{\alpha^2}{H_D}\right) - 2\rho_f\frac{\alpha}{H_D}. (15)$$

Taking the minus sign in Eq. (14) gives the so-called “fast-wave” slowness s_{Pf} and taking the plus sign gives the “slow-wave” slowness s_{Ps}. The remaining part of the linear poroelastic response due to the plane wave is given as

$$w_3 = \pm\beta U e^{i\omega[\pm s(\omega)x_3 - t]}, (16)$$

$$\tau_{33} = i\omega s(\omega)\,(H_U + \beta C)\,U e^{i\omega[\pm s(\omega)x_3 - t]}, (17)$$

$$-p_f = i\omega s(\omega)\,(C + \beta M)\,U e^{i\omega[\pm s(\omega)x_3 - t]}, (18)$$

where the parameter β is defined as

$$\beta = -\frac{H_U s^2 - \rho}{C s^2 - \rho_f}, (19)$$

and takes on different values for fast waves ($s = s_{Pf}$) and slow waves ($s = s_{Ps}$). Throughout the paper, we assume that linear response holds in the host poroelastic material and all nonlinear responses are due to the fracture.

B. Poroelastic linear-slip fracture-layer model

We now assume that there is an infinite fracture centered about the plane $x_3 = 0$ within an otherwise uniform and linear poroelastic host material. Real fractures consist of contacting asperities associated with the rough topography of the two fracture surfaces as shown in Fig. 1. Following Nakagawa and Schoenberg (2007), we assume that the fracture zone can be considered equivalent to a layer of highly compliant porous material having thickness *h* and approximated as having uniform properties. In future work, we plan to address the problem of allowing for the actual fracture surfaces with heterogeneous points of contact between them (Fig. 1), but for this work, we assume that representing the fracture as a compressible porous layer is an adequate approximation.

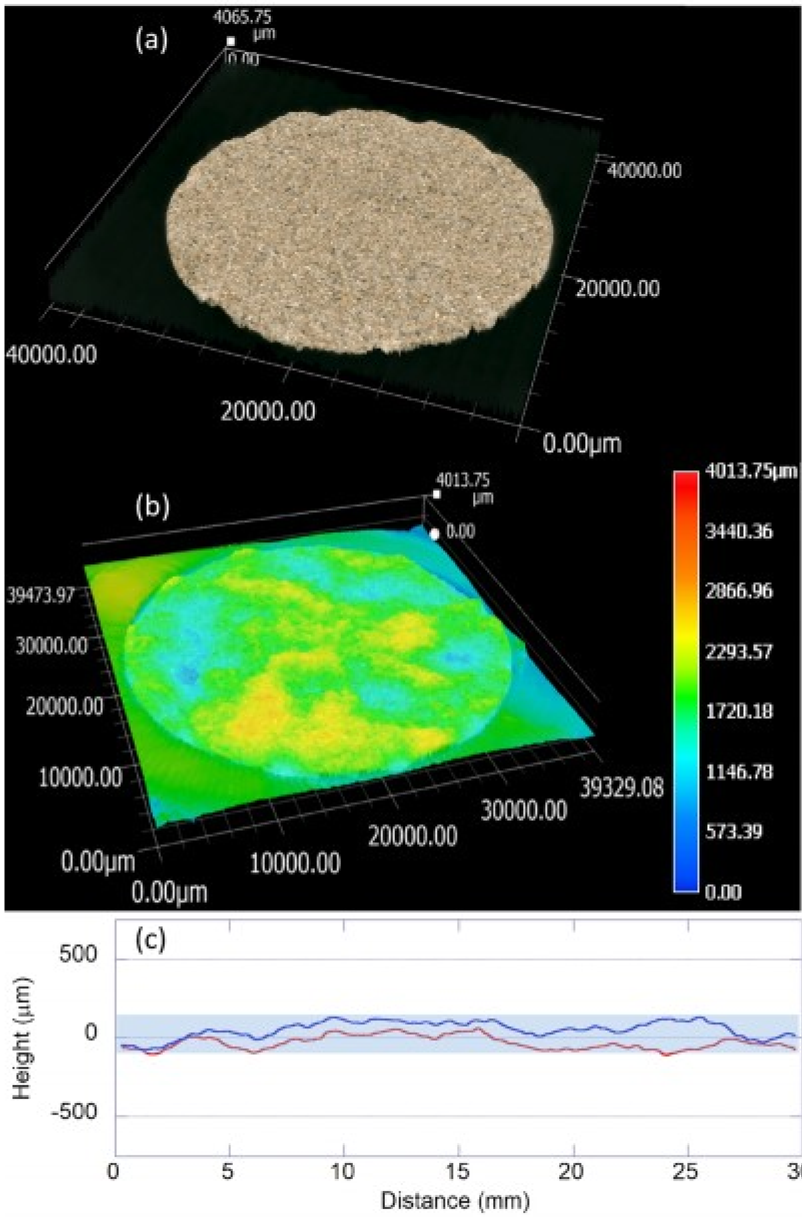

FIG. 1. (Color online) (a) A photograph of an actual fracture surface of Berea sandstone. (b) gives a color map of the topography of the same surface shown in (a). (c) is the measured aperture between the top (blue curve) and bottom (red curve) fracture surfaces along a linear cross section through the same fracture.

If the thickness *h* of the fracture layer is much smaller than the wavelengths of the plane waves propagating in the x_3 direction, we can take the strain within the fracture layer to be uniform and identify these strains as $d[u_3]/h = \partial du_3/\partial x_3$ and $d[w_3]/h = \partial dw_3/\partial x_3$, where

$d[u_3] = du_{3+}(x_3 = h/2) - du_{3-}(x_3 = -h/2)$ is the difference in the displacements between the top and bottom of the fracture layer. Plane longitudinal waves that are normally incident on the fracture layer, as depicted in Fig. 2, then satisfy the “jump” displacement conditions that come directly from the earlier compressibility laws of Eqs. (7) and (8) (Bakulin and Molotkov, 1997; Nakagawa and Schoenberg, 2007)

$$d\left[u_3\right] \equiv du_{3+} - (du_{3-} + du_{3I}) = \eta_D \left[d\tau - \alpha\,(-dp_f)\right], \quad (20a)$$

$$\begin{aligned} d\left[w_3\right] &\equiv dw_{3+} - (dw_{3-} + dw_{3I}) = -\alpha\, d\left[u_3\right] + \eta_M\,(-dp_f) \\ &= -\alpha\eta_D d\tau + (\eta_M + \alpha^2\eta_D)(-dp_f), \end{aligned} \quad (20b)$$

as well as the stress continuity conditions

$$d\tau_{33+} = d\tau_{33-} + d\tau_{33I} \equiv d\tau, \quad (21a)$$

$$dp_{f+} = dp_{f-} + dp_{fI} \equiv dp_f. \quad (21b)$$

In Eqs. (20a) and (20b), α is the Biot-Willis constant of the fracture layer, and the two fracture compliances η_D and η_M are defined as

$$\eta_D = \frac{h}{H_D} \quad \text{and} \quad \eta_M = \frac{h}{M}. \quad (22)$$

Note that the elastic moduli, such as H_D, M, and α, are for the fracture layer and are different from those of the background medium. To allow for linear scattering from the fracture, one assumes that the fracture compliances are not influenced by the wave stress and are given by the constant values $\eta_{D0} = h_0/H_{D0}$ and $\eta_{M0} = h_0/M_0$, corresponding to the fracture properties that hold prior to wave arrival. In this linear scattering case, the jump boundary conditions can be integrated to give

$$\left[u_3\right] = \eta_{D0}\left(\tau + \alpha_0 p_f\right), \quad (23a)$$

$$\left[w_3\right] = -\alpha_0\eta_{D0}\tau - (\eta_{M0} + \alpha_0^2\eta_{D0})p_f, \quad (23b)$$

where the integrated quantities u_3, w_3, τ, and p_f are the poroelastic wavefields in the linear theory. The above summarizes the linear-scattering theory of Nakagawa and Schoenberg (2007).

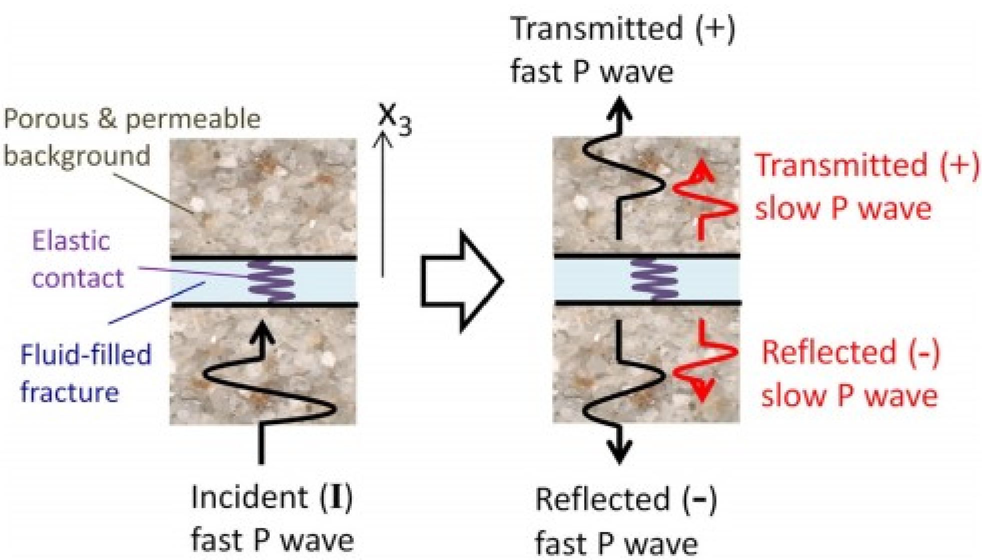

FIG. 2. (Color online) Plane wave incident (I) upon a fluid-filled fracture in a poroelastic medium generates transmitted (+) and reflected (−) fast and slow *P* waves.

C. General poroelastic nonlinear-slip fracture-layer model

For the remainder of this paper, we allow the integrated wavefield displacement discontinuities [u_3] and [w_3] to depend, in a nonlinear way, on the stress due to contact nonlinearity within the fracture. We neglect the impact of macroscopic fluid flow parallel to the extent of the fracture, which was considered by Nakagawa and Korneev (2014), because the incoming plane waves in this study are normally incident upon the fracture. Nonetheless, we assume that the fluid moves perpendicular to the fracture as characterized by w_3, which equilibrates the fluid pressure between the fracture and porous host so that the fluid pressure is continuous across the thin fracture aperture as indicated by Eq. (21b).

The nonlinearity in the displacement-discontinuity state functions can be expressed as [u_3] = $f(\tau, p_f)$ and [w_3] = $g(\tau, p_f)$. Although the functions f and g

can, in principle, be hysteretic if crack growth or loss processes are important as a wave interacts with a fracture, in the current analysis, we assume they are unique functions of the stress and fluid pressure, i.e., we only consider nonlinear “poroelastic” behavior. Assuming *f* and *g* are smooth differentiable functions, their bivariate Taylor series expansions about the stress state holding prior to wave arrival τ_0, p_{f0} are

$$\left[u_3\right](\tau, p_f) = f(\tau_0, p_{f0}) + \sum_{n=1}^{\infty} \frac{1}{n!} \sum_{k=0}^{n} \binom{n}{k} \left.\frac{\partial^n f}{\partial^{n-k}\tau\, \partial^k p_f}\right|_{\tau_0, p_{f0}} (\tau - \tau_0)^{n-k} \left(p_f - p_{f0}\right)^k, \tag{24a}$$

$$\left[w_3\right](\tau, p_f) = g(\tau_0, p_{f0}) + \sum_{n=1}^{\infty} \frac{1}{n!} \sum_{k=0}^{n} \binom{n}{k} \left.\frac{\partial^n g}{\partial^{n-k}\tau\, \partial^k p_f}\right|_{\tau_0, p_{f0}} (\tau - \tau_0)^{n-k} (p_f - p_{f0})^k, \tag{24b}$$

where the binomial coefficients are defined as usual by

$$\binom{n}{k} \equiv \frac{n!}{k!(n-k)!}.$$

In what follows, we define $[u_3]$ and $[w_3]$ to be zero prior to wave arrival, which amounts to working with $f(\tau_0, p_{f0}) = 0$ and $g(\tau_0, p_{f0}) = 0$ in whatever model we use for *f* and *g*. Upon defining $\delta\tau = \tau - \tau_0$ and $\delta p_f = p_f - p_{f0}$ as the possibly finite wave-induced stress deviations from the background state, we then have

$$\left[u_3\right] = \sum_{n=1}^{\infty} \frac{1}{n!} \sum_{k=0}^{n} \binom{n}{k} \left(\frac{\partial^n f}{\partial^{n-k}\tau \ \partial^k p_f} \right)_0 \delta\tau^{n-k} \delta p_f^k, (25a)$$

$$\left[w_3\right] = \sum_{n=1}^{\infty} \frac{1}{n!} \sum_{k=0}^{n} \binom{n}{k} \left(\frac{\partial^n g}{\partial^{n-k}\tau \ \partial^k p_f} \right)_0 \delta\tau^{n-k} \delta p_f^k. (25b)$$

The subscript “0” on the partial derivatives means they are being evaluated at the background stress state τ_0, p_{f0}.

Under these assumptions, the leading-order linear terms of these expansions are then

$$\left[u_3\right] \to \left(\frac{\partial f}{\partial \tau} \right)_0 \delta\tau + \left(\frac{\partial f}{\partial p_f} \right)_0 \delta p_f, (26a)$$

$$\left[w_3\right] \to \left(\frac{\partial g}{\partial \tau} \right)_0 \delta\tau + \left(\frac{\partial g}{\partial p_f} \right)_0 \delta p_f, (26b)$$

which correspond exactly to Eqs. (23a) and (23b). We may thus identify

$$\eta_{D0} = \left(\frac{\partial f}{\partial \tau} \right)_0, (27)$$

$$\alpha_0 = \left(\frac{\partial f / \partial p_f}{\partial f / \partial \tau} \right)_0 = -\left(\frac{\partial \tau}{\partial p_f} \right)_{[u_3]}, (28)$$

$$\eta_{M0} = -\left(\frac{\partial g}{\partial p_f} \right)_0 - \alpha_0^2 \eta_{D0} \ (29)$$

as being the fracture compliances in the Nakagawa and Schoenberg (2007) linear theory. We used a well-known fact of partial derivatives to write the second expression for α_0; this simply means that if $[u_3] = f(\tau, p_f)$ is not changing when there is an applied stress change $d\tau$, we must simultaneously apply a fluid-pressure change of $dp_f = -d\tau/\alpha_0$. The wavefield stress and pore-pressure continuity conditions are unchanged from the linear case in Eqs. (21a) and (21b); simply replace the infinitesimal d by the possibly finite wave perturbation "δ". We continue to use τ and p_f (the stress and pressure, respectively, which are continuous across the fracture) as convenient abbreviations for τ_{33+} and p_{f+}.

D. The highly compliant fracture-layer approximation

In principle, the nonlinear state functions f and g can be determined via extensive laboratory experiments and numerical simulations of a rough fracture interface for a range of τ and p_f. To simplify the situation, we assume that the equivalent fracture layer is much more compliant than the surrounding host material. Specifically, we make the approximation that the fracture layer has a Biot-Willis coefficient given as $\alpha \approx 1$, which corresponds to $K_D/K_s \ll 1$. This will simplify much of the analysis while still allowing for a realistic nonlinear fracture response. Note as well that for the fracture layer, the changes $d[u_3]$ of the jump in solid displacements is exactly given by $d[u_3] = dh$, which upon integration gives $[u_3] = h - h_0$ where h_0 is the fracture aperture at the background stress state, a fact to be used throughout what follows.

1. The wave-induced fracture opening $[u_3]$

When $\alpha = 1$ in the fracture layer, the jump condition becomes $d[u_3] = \eta_D d(\tau + p_f)$. Integrating this yields $[u_3] = f(\delta\tau^*)$ where $\delta\tau^* = \tau - \tau_0 + p_f - p_{f0}$ is the wave-induced effective stress. So under the highly compliant fracture assumption, the nonlinear wave-stress dependence of $[u_3]$ is given as

$$\left[u_3\right] = \sum_{n=1}^{\infty} \frac{1}{n!}\left(\frac{d^n f}{d\tau^{*n}}\right)_0 \delta\tau^{*n}. (30)$$

To proceed, specific forms for the stress dependence of $[u_3]$ are required.

Although the nonlinear poroelastic function $f(\tau, p_f)$ for a fluid-saturated fracture has never been experimentally or numerically explored as a function of both τ and p_f, a dry fracture embedded in an elastic solid has received considerable attention. For example, Goodman *et al.* (1968) and Goodman (1976) propose a generalized hyperbolic model describing the deformation of a dry fracture as a function of the stress for a wide range of fracture surface topographies and stress histories (Bandis *et al.*, 1983). Detournay (1979) proposes a semi-logarithmic model that shows a good fit to the initial normal deformation of displaced (sheared) rough surfaces (e.g., Lang *et al.*, 2016;

Zangerl *et al.*, 2008). Biwa *et al.* (2004) examine nonlinear scattering of waves from a dry fracture embedded in an elastic host using a power-law model, which includes the semi-logarithmic model as a special case.

When the compliant-fracture assumption built into Eq. (30) is valid, fracture aperture at any pore pressure can be predicted using the effective stress $\tau^* = \tau + p_f$. For example, if a semi-logarithmic fracture deformation model is used, the fracture closure function is

$$\left[u_3\right] = \tau_0^* \ \eta_{D0} \ \ln\left(1 + \frac{\delta\tau^*}{\tau_0^*}\right) = \tau_0^* \ \eta_{D0} \ \ln\left(\frac{\tau^*}{\tau_0^*}\right), (31)$$

and the drained specific normal fracture compliance is determined as

$$\eta_D = \frac{d[u_3]}{d(\delta\tau^*)} = \frac{d[u_3]}{d\tau^*} = \frac{\eta_{D0}}{1 + \delta\tau^*/\tau_0^*} = \frac{\eta_{D0}\tau_0^*}{\tau^*}, (32)$$

where we used that $d(\delta\tau^*) = d(\tau^* - \tau_0^*) = d\tau^*$ because τ_0^* is not changing on the time scale of the seismic wave passage. Such a model makes explicit how either $[u_3]$ or η_D depends, in a nonlinear way, on the varying effective stress level τ^*.

For more general effective-stress dependence in the fracture closure $[u_3]$ model we can use a series in the dimensionless form

$$\frac{[u_3]}{h_0} = \frac{\delta\tau^*}{h_0/\eta_{D0}} \sum_{n=1}^{\infty} C_n \left(\frac{\delta\tau^*}{\sigma}\right)^{n-1}, (33)$$

where σ is the positive amplitude of the effective stress present prior to wave arrival. Because the fracture needs to be in a compressed state in order for the asperities to be in contact and have a finite compliance, we have $\sigma = -\tau_0^*$ because τ^* is negative in a state of compression. Note that $C_1 = 1$ because $(\partial[u_3]/\partial\tau^*)_{\delta\tau^*=0} = \eta_{D0}$.

We now introduce a small dimensionless parameter $\varepsilon = \delta\tau^*_{\max}/\sigma$, which will be the expansion parameter in the perturbation analysis that follows, where $\delta\tau^*_{\max}$ is the maximum amplitude of the wave-induced effective stress acting in the porous material without a fracture present. We can further write

$$\frac{\delta\tau^*}{h_0/\eta_{D0}} = \frac{\delta\tau^*}{\delta\tau^*_{\max}} \frac{\delta\tau^*_{\max}}{\sigma} \frac{\sigma}{h_0/\eta_{D0}}, (34)$$

where the quantity h_0/η_{D0} is again the effective drained uniaxial modulus of the compliant fracture (measured in Pa). Because the fracture is being taken to be much more compliant than the porous host material, we will assume that the dimensionless parameter

$$c_\eta = \frac{\sigma}{h_0/\eta_{D0}} (35)$$

is closer to $O(1)$ in what follows than to $O(\varepsilon)$. As such, Eq. (33) can be written in the final compact form

$$\frac{[u_3]}{h_0} = c_\eta \sum_{n=1}^{\infty} C_n \varepsilon^n \left(\frac{\delta\tau^*}{\delta\tau_{\max^*}} \right)^n, (36)$$

where all terms are $O(1)$ other than the powers of ε explicitly present. For the particular case of the semi-logarithmic fracture function given in Eq. (31), a Taylor-series expansion yields $C_n = 1/n$ exactly in Eq. (36).

2. The relative fluid displacement from the fracture *[*w_3*]*

In this section, we derive a series expansion of the finite Darcy displacement $[w_3]$ that characterizes how the displacement of the fluid out of the fracture and into the porous host depends, in a nonlinear way, on both the wave-induced effective stress $\delta\tau^* = \tau^* - \tau^*_0$ and the wave-induced fluid pressure $\delta p_f = p_f - p_{f0}$. This jump condition involving the relative fluid-solid displacements w_3 perpendicular to the fracture must describe the conservation of fluid mass. As such, $d(\rho_f[w_3])$ represents the incremental change in fluid mass due to fluid mass fluxing out of the fracture into the porous host, and must be equal to the decrease of the fluid mass within the fracture $-d(\rho_f\phi h)$, where h is the fracture aperture and ϕ is the porosity within the fracture layer. Upon equating these two expressions, we have

$$d(\rho_f[w_3]) = -d(\rho_f \phi h), (37)$$

which is then integrated from the reference state prior to wave arrival characterized by ρ_{f0}, ϕ_0, and h_0 yielding

$$\rho_f[w_3] = -\rho_f \phi h + \rho_{f0}\phi_0 h_0. (38)$$

To understand how porosity evolves in the fracture due to wave stress, we again assume the fracture layer is a Gassmann material for which the porosity changes according to Eq. (12). Using the highly compliant fracture approximation that $\alpha = 1 - K_D/K_s \approx 1$ then gives the porosity change as

$$d\phi = \frac{(1-\phi)}{H_D} d\tau^*, (39)$$

where again $d\tau^* = d\tau + dp_f$. Because $d[u_3]/h = dh/h = d\tau^*/H_D$, Eq. (39) can be rewritten as

$$\frac{d(1-\phi)}{1-\phi} = -\frac{dh}{h}, (40)$$

which then integrates from the reference state to give

$$\phi h = \phi_0 h_0 + [u_3]. (41)$$

Because $[u_3] = h - h_0$, this result can also be written $h(1 - \phi) = h_0(1 - \phi_0)$, which is the statement that solid volume within the deforming fracture remains constant during wave passage and is a consequence of our assuming that $K_D/K_s \rightarrow 0$. We thus can write Eq. (38) in the form

$$\frac{[w_3]}{h_0} = -\frac{[u_3]}{h_0} - \phi_0\left(1 - \frac{\rho_{f0}}{\rho_f}\right). (42)$$

To proceed further, a model for how the fluid density ρ_f depends on the wave-induced fluid pressure is required.

To allow for a range of fluid scenarios, we assume the fluid is a liquid that possibly has small gas bubbles within it. The liquid is characterized by a bulk modulus K_ℓ that is taken to be independent of pressure, i.e., $K_\ell = K_{\ell 0}$ is a constant during wave passage. The gas is taken to be ideal and undergoes isentropic (adiabatic and reversible) changes, which means it has the bulk modulus $K_g = \gamma p_g$, where p_g is the gas pressure and γ is the adiabatic index. For diatomic molecules, such as nitrogen and oxygen, $\gamma = 1.4$. We assume the surface tension of the gas bubbles is negligible so that the pressure throughout the liquid and gas is the same, i.e., $p_g = p_\ell = p_f$. Initially, before the arrival of the wave, we characterize the volume fraction of gas as v_{g0} and the volume fraction of liquid as $v_{\ell 0}$ where $v_{g0} + v_{\ell 0} = 1$.

The volume of gas at any moment during wave passage V_g is obtained by integrating $dV_g/V_g = -dp_f/(\gamma p_f)$ to give $V_g = v_{g0}V_0(p_{f0}/p_f)^{1/\gamma}$, where $v_{g0}V_0$ is the volume of gas initially present in a volume V_0 of fluid prior to wave arrival. The volume of liquid at any moment during wave passage V_ℓ is obtained by integrating $dV_\ell/V_\ell = -dp_f/K_{\ell 0}$ to give $V_\ell = v_{\ell 0} V_0 \, \exp\left\{-\left(p_f - p_{f0}\right)/K_{\ell 0}\right\}$. Thus, the total volume of fluid that is changing during wave passage is $V = V_g + V_\ell$, which when divided by the constant mass M of the fluid gives the density model

$$\frac{V}{V_0} = \frac{M}{V_0}\frac{V}{M} = \frac{\rho_{f0}}{\rho_f} = v_{g0}\left(\frac{p_{f0}}{p_f}\right)^{1/\gamma} + v_{\ell 0} e^{-(p_f - p_{f0})/K_{\ell 0}}, \quad (43)$$

which in terms of the wave-induced fluid pressure variable $\delta p_f = p_f - p_{f0}$ can be written as

$$\frac{\rho_{f0}}{\rho_f} = \frac{v_{g0}}{\left(1 + \delta p_f/p_{f0}\right)^{1/\gamma}} + v_{\ell 0} e^{-\delta p_f/K_{\ell 0}}. \quad (44)$$

This will be our model for how ρ_{f0}/ρ_f depends on the wave-induced fluid pressure δp_f.

The function $-(1 - \rho_{f0}/\rho_f)$ required in Eq. (42) can be expanded in terms of powers of ε to yield the series

$$-\left(1 - \frac{\rho_{f0}}{\rho_f}\right) = v_{g0}\sum_{n=1}^{\infty}\frac{(-1)^n}{n!}F_n\varepsilon^n\left(c_g\frac{\delta p_f}{\delta\tau^*_{\max}}\right)^n + v_{\ell 0} \sum_{n=1}^{\infty}\frac{(-1)^n}{n!}\varepsilon^{2n}\left(c_\ell\frac{\delta p_f}{\delta\tau^*_{\max}}\right)^n, \quad (45)$$

where

$$F_n \equiv \begin{cases} 1, & n = 0, \\ \frac{1 \cdot 1 \cdot (1+\gamma)(1+2\gamma) \cdots [1+(n-1)\gamma]}{\gamma^n}, & n > 0, \end{cases} \quad (46)$$

and we have introduced $O(1)$ dimensionless parameters c_ℓ and c_g as

$$c_\ell = \frac{\sigma^2}{\delta\tau^*_{\max} K_{\ell 0}}, \quad c_g = \frac{\sigma}{p_{f0}}, \quad (47)$$

which assume that the ratio of the background effective stress σ to bulk modulus of the liquid $K_{\ell 0}$ is small and of order $\varepsilon = \delta\tau^*_{\max}/\sigma$ (the perturbation parameter).

Looking ahead to the perturbation analysis of the nonlinear wave scattering analysis, and noting that we will only need results through $O(\varepsilon^4)$, the final result for $[w_3]$ that will be needed is

$$\frac{[w_3]}{h_0} = -\frac{[u_3]}{h_0} + \sum_{n=1}^{4} D_n \left(\frac{\delta p_f}{\delta\tau^*_{\max}} \right)^n, (48)$$

where the dimensionless but ε-dependent coefficients D_n are defined through $O(\varepsilon^4)$ as

$$D_1(\varepsilon) = -\phi_0 \left(v_{g0} c_g F_1 \varepsilon + v_{l0} c_\ell \varepsilon^2 \right), (49a)$$

$$D_2(\varepsilon) = \phi_0 \left(v_{g0} c_g^2 F_2 \varepsilon^2 + v_{l0} c_\ell^2 \varepsilon^4 / 2 \right), (49b)$$

$$D_3(\varepsilon) = -\phi_0 v_{g0} c_g^3 F_3 \varepsilon^3, (49c)$$

$$D_4(\varepsilon) = \phi_0 v_{g0} c_g^4 F_4 \varepsilon^4, (49d)$$

which reveal that there is a different ε dependence in the cases of $v_{g0} \neq 0$ compared to $v_{g0} = 0$ due to gas being more sensitive to fluid-pressure changes than liquid.

The first coefficient D_1 in Eq. (49a), which is involved in the leading-order (linear) scattering from the fracture, can be rewritten using the bulk modulus of the gas-liquid mixture at the resting state $K_{f0} = (v_{g0}/\gamma p_{f0} + v_{\ell 0}/K_{\ell 0})^{-1}$ as

$$D_1(\varepsilon) = -\phi_0 \sigma \left(\frac{v_{g0}}{\gamma p_{f0}} + \frac{v_{\ell 0}}{K_{\ell 0}} \right) \varepsilon = -\frac{\sigma \phi_0}{K_{f0}} \varepsilon = -c_\mu \varepsilon, (50)$$

where a new $O(1)$ dimensionless coefficient

$$c_\mu = \frac{\sigma \phi_0}{K_{f0}} = \sigma \phi_0 \left(\frac{v_{g0}}{\gamma p_{f0}} + \frac{v_{\ell 0}}{K_{\ell 0}} \right) (51)$$

was introduced. Note as well that from Eq. (48), the fluid-storage fracture compliance η_{M0} in the above highly compliant ($\alpha = 1$) fracture model is

$$\eta_{M0} = -\left(\frac{\partial [w_3]}{\partial p_f} \right)_0 = \frac{h_0 \phi_0}{K_{f0}} = \frac{h_0}{M_0}, (52)$$

where $M_0 = K_{f0}/\phi_0$ is the fluid-storage coefficient of the fracture layer prior to wave arrival.

E. Application of a perturbation method

From here on, we analyze the nonlinear scattering of waves from the fracture. As such, all stress, fluid pressure, and displacement variables are understood to be those associated with the waves and not the initial state, which held prior to wave arrival at the fracture. We thus define dimensionless-and-$O(1)$ effective stress τ_e and fluid pressure p wavefield variables as

$$\tau_e \equiv \frac{\delta \tau^*}{\delta \tau^*_{\max}} = \frac{\tau - \tau_0 + p_f - p_{f0}}{\delta \tau^*_{\max}}, (53)$$

$$p \equiv \frac{\delta p_f}{\delta \tau^*_{\max}} = \frac{p_f - p_{f0}}{\delta \tau^*_{\max}}, (54)$$

it being understood that the new variables τ_e and p are zero prior to wave arrival. Next, because $[u_3]$ and $[w_3]$ are both $O(\varepsilon)$ from Eqs. (36) and (48), we further rewrite the displacement-jump variables as the dimensionless $O(1)$ quantities

$$\left[u\right] \equiv \frac{[u_3]}{h_0\varepsilon} = \frac{[u_3]}{h_0\delta\tau^*_{\max}/\sigma}, (55)$$

$$\left[w\right] \equiv \frac{[w_3]}{h_0\varepsilon} = \frac{[w_3]}{h_0\delta\tau^*_{\max}/\sigma}. (56)$$

In terms of these rescaled wavefield variables, the poroelastic nonlinear jump-displacement boundary conditions for a thin fracture can be written as

$$\left[u\right] = u_+ - u_- - u_I = c_\eta \sum_{n=1}^{4} C_n \varepsilon^{n-1}\tau_e^n + O(\varepsilon^4), (57a)$$

$$\left[w\right] = w_+ - w_- - w_I = -\left[u\right] + \sum_{n=1}^{4} \frac{D_n(\varepsilon)}{\varepsilon} p^n + O(\varepsilon^4), (57b)$$

along with the stress continuity conditions

$$\tau_{e+} = \tau_{e-} + \tau_{eI} \equiv \tau_e, (58a)$$

$$p_+ = p_- + p_I \equiv p. (58b)$$

The variables having the subscripts +, –, and I (standing for forward- and backward-propagating waves and forward-propagating incident waves in the x_3 direction, respectively) have also been converted into dimensionless $O(1)$ variables.

To apply a perturbation approach (e.g., Nayfeh, 2007) for solving the planewave scattering problem involving the nonlinear boundary conditions of Eqs. (57a) and (58b), we express the displacements and stresses as perturbation series using the ansatz

$$X(t) = \sum_{n=0}^{3} \varepsilon^n X^{(n)}(t), (59)$$

where X represents any of the suite of variables $u_\pm$, $w_\pm$, $\tau_{e\pm}$, and $p_\pm$. Because we will be examining the response only through $n = 3$, we only need the following orders of the powers of the transmitted stress variables:

$$p = p^{(0)} + p^{(1)}\varepsilon + p^{(2)}\varepsilon^2 + p_f^{(3)}\varepsilon^3, (60a)$$

$$p^2 = p^{(0)2} + 2p^{(0)}p^{(1)}\varepsilon + \left(2p^{(0)}p^{(2)} + p^{(1)2}\right)\varepsilon^2, (60b)$$

$$p^3 = p^{(0)3} + 3p^{(0)2}p^{(1)}\varepsilon, (60c)$$

$$p^4 = p^{(0)4}, (60d)$$

with equivalent expressions for the powers of τ_e.

By equating terms of the same powers of ε, the boundary conditions can then be rewritten

$$u_+^{(n)} - u_-^{(n)} = u_I^{(n)} + c_\eta \tau_e^{(n)}, (61a)$$

$$w_+^{(n)} - w_-^{(n)} = w_I^{(n)} - c_\eta \tau_e^{(n)} - c_\mu p^{(n)}, (61b)$$

$$\tau_e^{(n)} = \tau_{e-}^{(n)} + \delta_{n0}\tau_{eI}, (61c)$$

$$p^{(n)} = p_-^{(n)} + \delta_{n0} p_I. (61d)$$

The leading order n = 0 corresponds to linear scattering off the fracture. Nonlinear effects begin at n = 1.

The $u_I^{(n)}$ and $w_I^{(n)}$ are the source terms generating the scattering at each order n and are given by

$$u_I^{(0)} = u_I, \text{(62a)}$$

$$u_I^{(1)} = c_\eta C_2 \tau^{(0)2}, \text{(62b)}$$

$$u_I^{(2)} = c_\eta \left(2C_2 \tau_e^{(0)} \tau_e^{(1)} + C_3 \tau_e^{(0)3}\right), \text{(62c)}$$

$$u_I^{(3)} = c_\eta \left[C_2 \left(2\tau_e^{(0)} \tau_e^{(2)} + \tau_e^{(1)2}\right) + 3C_3 \tau_e^{(0)2} \tau_e^{(1)} + C_4 \tau_e^{(0)4}\right], \text{(62d)}$$

And

$$w_I^{(0)} = w_I, \text{(63a)}$$

$$w_I^{(1)} = -u_I^{(1)} + v_{g0}\phi_0 c_g^2 F_2 p^{(0)2}, \text{(63b)}$$

$$w_I^{(2)} = -u_I^{(2)} + v_{g0}\phi_0 \left(2c_g^2 F_2 p^{(0)} p^{(1)} - c_g^3 F_3 p^{(0)3}\right), \text{(63c)}$$

$$\begin{aligned} w_I^{(3)} &= -u_I^{(3)} \\ &+ v_{g0}\phi_0\left[c_g^2 F_2 \left(2p^{(0)} p^{(2)} + p^{(1)2}\right) - 3c_g^3 F_3 p^{(0)2} p^{(1)} + c_g^4 F_4 p^{(0)4}\right] \\ &+ v_{\ell 0}\phi_0 \frac{c_\ell^2 p^{(0)2}}{2}. \end{aligned} \qquad \text{(63d)}$$

The liquid is having an effect on the linear scattering through the $c_\mu = \sigma/K_{f0}$ coefficient in Eq. (61b). However, the first nonlinear influence of the liquid on the scattering occurs in the source term of Eq. (63d), which is why we took the analysis through to n = 3 effects.

For the various forward- and backward-propagating fast- and slow-compressional plane waves in the porous host on either side of the fracture located at $x_3 = 0$, the displacement and stress response associated with each wave type are related to each other as given earlier by Eqs. (13)–(19). Expressing the solid displacement amplitudes of each planewave type at each perturbation order n as $U = \pm a^{(n)}_{P_f\pm,P_s\pm}$, we obtain

$$\boldsymbol{u}^{(n)}_{\pm}(\omega) \equiv \begin{bmatrix} u^{(n)}_{\pm} \\ w^{(n)}_{\pm} \end{bmatrix} = \pm \begin{bmatrix} 1 & 1 \\ \beta_{Pf} & \beta_{Ps} \end{bmatrix} \begin{bmatrix} a^{(n)}_{Pf\pm} \\ a^{(n)}_{Ps\pm} \end{bmatrix} e^{-i\omega t} \equiv \pm \widehat{\boldsymbol{U}}(\omega) \cdot \boldsymbol{a}^{(n)}_{\pm} e^{-i\omega t}, \tag{64a}$$

$$\boldsymbol{\tau}^{(n)}_{e\pm}(\omega) \equiv \begin{bmatrix} \tau^{(n)}_{e\pm} \\ -p^{(n)}_{\pm} \end{bmatrix} = i\omega F_\sigma \begin{bmatrix} H_U - C & C - M \\ C & M \end{bmatrix} \cdot \begin{bmatrix} 1 & 1 \\ \beta_{Pf} & \beta_{Ps} \end{bmatrix} \begin{bmatrix} s_{P_f} & 0 \\ 0 & s_{P_s} \end{bmatrix} \begin{bmatrix} a^{(n)}_{Pf\pm} \\ a^{(n)}_{Ps\pm} \end{bmatrix} e^{-i\omega t} \equiv i\omega \boldsymbol{Z}(\omega) \cdot \boldsymbol{a}^{(n)}_{\pm} e^{-i\omega t}. \tag{64b}$$

A dimensionless displacement matrix $\widehat{\boldsymbol{U}}(\omega)$ and impedance matrix $\boldsymbol{Z}(\omega)$ have been introduced through these relations. The coefficient

$$F_\sigma \equiv \frac{h_0 \varepsilon}{\delta \tau^*_{\max}} = \frac{h_0}{\sigma} \tag{65}$$

results from the use of dimensionless stress and displacement variables. The various material properties in the displacement and stress response of Eqs. (64a) and (64b) are those of the host linear-poroelastic material.

The vector-matrix form of the boundary conditions in Eqs. (61a)–(61d) are

$$\boldsymbol{u}_{+}^{(n)} - \boldsymbol{u}_{-}^{(n)} - \boldsymbol{u}_{I}^{(n)} = \boldsymbol{\eta} \cdot \boldsymbol{\tau}_{e+}^{(n)}, \text{(66a)}$$

$$\boldsymbol{\tau}_{e+}^{(n)} = \boldsymbol{\tau}_{e-}^{(n)} + \delta_{n0}\boldsymbol{\tau}_{eI}, \text{(66b)}$$

where a dimensionless fracture compliance matrix is defined as

$$\boldsymbol{\eta} \equiv \begin{bmatrix} c_\eta & 0 \\ -c_\eta & c_\mu \end{bmatrix} = F_\sigma^{-1} \begin{bmatrix} \eta_{D0} & 0 \\ -\eta_{D0} & \eta_{M0} \end{bmatrix}. \text{(67)}$$

By introducing Eqs. (64a) and (64b) into Eqs. (66a) and (66b), we obtain

$$\begin{aligned} \boldsymbol{a}_{+}^{(n)} &= \left[2\widehat{\boldsymbol{U}}(\omega) - i\omega\boldsymbol{\eta} \cdot \mathbf{Z}(\omega)\right]^{-1} \\ &\cdot \left\{\boldsymbol{u}_{I}^{(n)} + \delta_{n0}\widehat{\boldsymbol{U}}(\omega) \cdot [i\omega\mathbf{Z}(\omega)]^{-1} \cdot \boldsymbol{\tau}_{eI}\right\} e^{+i\omega t}, \end{aligned} \text{(68a)}$$

$$\boldsymbol{a}_{-}^{(n)} = \boldsymbol{a}_{+}^{(n)} - \delta_{n0}[i\omega\mathbf{Z}(\omega)]^{-1} \cdot \boldsymbol{\tau}_{eI}e^{+i\omega t}. \text{(68b)}$$

Equations (68a) and (68b) are used in Eqs. (64a) and (64b) to compute the displacement and stress for a range of frequencies for the *n*th-order nonlinear perturbation problem, which are subsequently collected and used to compute the time-domain stress (and pressure) waves at order *n*. The waves obtained from the lower-order problems are then combined to compute the nonlinear source terms for the next higher-order in the *n* scattering problem. The source term is transformed into the frequency domain, and the linear solutions for a range of frequencies are obtained from Eqs. (68a) and (68b) for the (*n*+1)th-order problem. This iterative process of transforming between the frequency domain and time domain at each order *n* of scattering is depicted in Fig. 3.

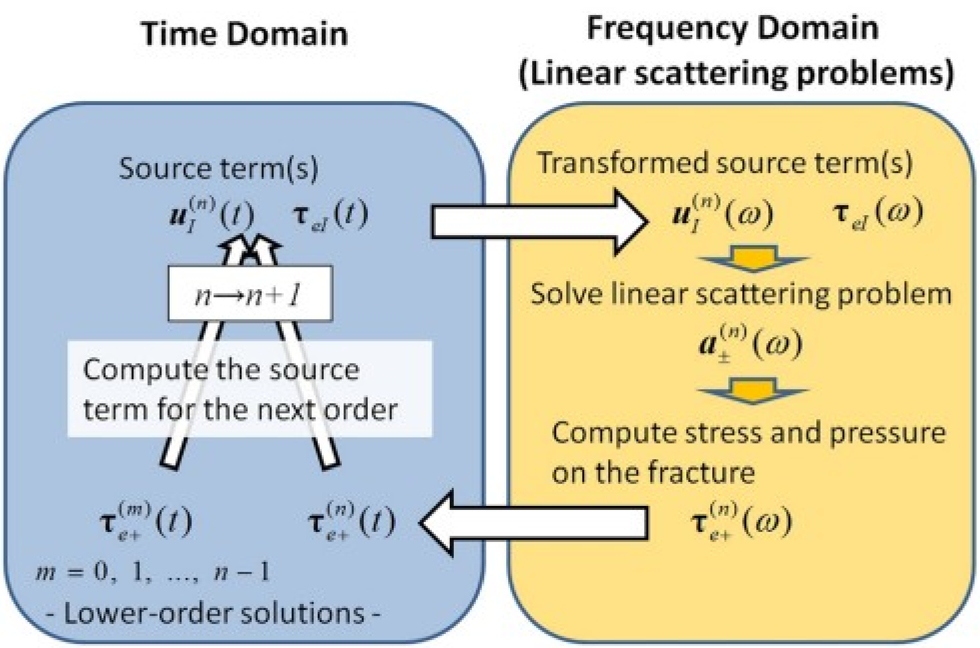

FIG. 3. (Color online) Iterative solution of a perturbation problem. For a given source term, the scattering problem can be solved in the frequency domain. The determined stress (and pressure) on the fracture is transformed back to the time domain to compute the $(n + 1)$th-order source term, combined with the lower-order solutions. Note that the stress source term is needed only for the zeroth-order problem.

Particularly for $n = 0$ (linear scattering), the displacement and stress for the incident wave are given via the incident wave's coefficient vector $\boldsymbol{a}_I$ as

$$\boldsymbol{u}_I = U_I^{(0)} = \widehat{\boldsymbol{U}}(\omega) \cdot \boldsymbol{a}_I e^{-i\omega t}, \tag{69a}$$

$$\boldsymbol{\tau}_{eI} = i\omega \mathbf{Z}(\omega) \cdot \boldsymbol{a}_I e^{-i\omega t}. \tag{69b}$$

By introducing Eqs. (69a) and (69b) into Eqs. (68a) and (68b), zeroth-order complex transmission and reflection coefficient matrices $\boldsymbol{T}^{(0)}$ and $\boldsymbol{R}^{(0)}$ can be computed via

$$a_{+}^{(0)} = 2\left[2\widehat{\boldsymbol{U}}(\omega) - i\omega\boldsymbol{\eta}\cdot\boldsymbol{Z}(\omega)\right]^{-1}\cdot\widehat{\boldsymbol{U}}(\omega)\cdot\boldsymbol{a}_I \equiv \boldsymbol{T}^{(0)}(\omega)\cdot\boldsymbol{a}_I, \quad (70a)$$

$$\boldsymbol{a}_{-}^{(0)} = \left(\boldsymbol{T}^{(0)} - \boldsymbol{I}\right)\cdot\boldsymbol{a}_I \equiv \boldsymbol{R}^{(0)}\cdot\boldsymbol{a}_I. \quad (70b)$$

Note that $\boldsymbol{T}^{(0)}(0) = \boldsymbol{I}$ (identity matrix) and $\boldsymbol{R}^{(0)}(0) = \boldsymbol{0}$.

F. Single-frequency solution for the nonlinear scattering of an incident fast *P* wave

As a special case, we examine the scattering of an incident fast *P* wave consisting of a cosine wave with a circular frequency ω. The rescaled displacement [Eq. (62a)] and Darcy flux [Eq. (63a)] of the incident waves on the fracture are given by

$$\begin{bmatrix} u_I^{(0)} \\ w_I^{(0)} \end{bmatrix} = |u_I|\begin{bmatrix} \cos(-\omega t) \\ |\beta_{Pf}(\omega)| \cos(-\omega t + \varphi_0) \end{bmatrix} \quad (71)$$
$$= \widehat{\boldsymbol{U}}(-\omega)\cdot\boldsymbol{a}_I(-\omega)e^{i\omega t} + \widehat{\boldsymbol{U}}(\omega)\cdot\boldsymbol{a}_I(\omega)e^{-i\omega t},$$

where $\boldsymbol{a}_I(\pm\omega) = [|u_I|/2 \quad 0]^T$, and $|u_I|$ is the amplitude of the solid frame displacement of the incident fast *P* wave. The phase delay φ_0 is given by the function $\beta_{Pf}(\omega)$ so that $\beta_{Pf}(\omega) = |\beta_{Pf}(\omega)| \exp(i\varphi_0)$. Note that, for real-valued wave displacement in the time domain, $\beta_{Pf}(-\omega) = \overline{\beta_{Pf}(\omega)}$ and $\varphi_0(-\omega) = -\varphi_0(\omega)$ where "$\bar{\ }$" indicates complex conjugation.

The coefficients of the zeroth-order transmitted and reflected wave displacements, $\boldsymbol{a}_{\pm}^{(0)}$, are computed from Eqs. (70a) and (70b) for the two frequencies $\pm\omega$. From these, the displacements of the transmitted and reflected waves are obtained via Eq. (64a) as

$$\boldsymbol{u}_+^{(0)}(t) = \widehat{\boldsymbol{U}}(-\omega) \cdot \boldsymbol{a}_+^{(0)}(-\omega)e^{i\omega t} + \widehat{\boldsymbol{U}}(\omega) \cdot \boldsymbol{a}_+^{(0)}(\omega)e^{-i\omega t}$$
$$= |u_I| \,\mathbf{Re}\left\{\widehat{\boldsymbol{U}}(\omega) \cdot \boldsymbol{T}^{(0)}(\omega)e^{-i\omega t}\right\} \cdot \begin{bmatrix} 1 \\ 0 \end{bmatrix}, \tag{72a}$$

$$\boldsymbol{u}_-^{(0)}(t) = \widehat{\boldsymbol{U}}(-\omega) \cdot \boldsymbol{a}_-^{(0)}(-\omega)e^{i\omega t} + \widehat{\boldsymbol{U}}(\omega) \cdot \boldsymbol{a}_-^{(0)}(\omega)e^{-i\omega t}$$
$$= |u_I| \,\mathbf{Re}\left\{\widehat{\boldsymbol{U}}(\omega) \cdot \boldsymbol{R}^{(0)}(\omega)e^{-i\omega t}\right\} \cdot \begin{bmatrix} 1 \\ 0 \end{bmatrix}. \tag{72b}$$

The symbol “**Re**” indicates the real-value part of the evaluated quantity.

The effective stress and fluid pressure on the fracture are, using Eq. (64b),

$$\begin{bmatrix} \tau_{e+}^{(0)}(t) \\ -p_+^{(0)}(t) \end{bmatrix} = i\omega \boldsymbol{Z}(\omega) \cdot \boldsymbol{a}_+^{(0)}(\omega)e^{-i\omega t} + i(-\omega)\boldsymbol{Z}(-\omega) \cdot \boldsymbol{a}_+^{(0)}(-\omega)e^{i\omega t}$$
$$\equiv |u_I| \begin{bmatrix} |\kappa_{\tau_0}| \;\cos\,(-\omega t + \varphi_{\tau_0}) \\ |\kappa_{p_0}| \;\cos\,(-\omega t + \varphi_{p_0}) \end{bmatrix}, \tag{73}$$

where we introduced complex unit amplitude responses κ_{τ_0} and κ_{p_0}, and their phases φ_{τ_0} and φ_{p_0}. Note that, although we shall not indicate so explicitly, these are dependent upon the frequency of the incident wave ω.

The nonlinear source terms for the first-order equations in Eqs. (62b) and (63b) are

$$u_I^{(1)} = \frac{c_\eta C_2}{2}|u_I|^2|\kappa_{\tau_0}|^2\left[1 + \cos\,(-2\omega t + 2\varphi_{\tau_0})\right], \tag{74a}$$

$$w_I^{(1)} = -u_I^{(1)} + \frac{v_{g0}\phi_0 c_g^2 F_2}{2}|u_I|^2|\kappa_{p_0}|^2\left[1 + \cos\,(-2\omega t + 2\varphi_{p_0})\right]. \tag{74b}$$

Note that the cosine terms in Eqs. (74a) and (74b) have two Fourier components $e^{i2\omega t}$ and $e^{-i2\omega t}$. Also, the time-independent terms indicate static fracture aperture changes. Korshak *et al.* (2002) discussed this phenomenon for elastic fractures and provided laboratory observations. These are the direct consequences of the interactions (multiplications) between two harmonic waves in the source, $\tau_{e+}^{(0)}(t)^2$ and $p_+^{(0)}(t)^2$, producing a difference-frequency [$\omega - \omega = 0$ (static)] wave and sum-frequency waves ($\omega + \omega = 2\omega$). Also note that if the source function contains multiple frequency components, for example, ω_1 and ω_2, the scattered waves contain both sum and difference frequencies $\omega_1 \pm \omega_2$.

Because the boundary conditions in Eqs. (61a)–(61d) for each order of perturbation are linear except for the source term, the plane wave scattering problem can be solved for each frequency of the nonlinear source term. For the current problem, these are 0 (static), -2ω, and $+2\omega$. From Eqs. (68a) and (68b),

$$\boldsymbol{a}_+^{(1)}(0) = \boldsymbol{a}_-^{(1)}(0) = (1/2)\widehat{\boldsymbol{U}}(0)^{-1} \cdot \boldsymbol{u}_I^{(1)}(0), \quad \text{(75a)}$$

$$\begin{aligned} \boldsymbol{a}_+^{(1)}(\pm 2\omega) &= \boldsymbol{a}_-^{(1)}(\pm 2\omega) \\ &= \left[2\widehat{\boldsymbol{U}}(\pm 2\omega) \mp i2\omega\boldsymbol{\eta} \cdot \boldsymbol{Z}(\pm 2\omega)\right]^{-1} \cdot \boldsymbol{u}_I^{(1)}(\pm 2\omega) \quad \text{(75b)} \\ &= (1/2)\widehat{\boldsymbol{U}}(\pm 2\omega)^{-1} \cdot \boldsymbol{S}(\pm 2\omega) \cdot \boldsymbol{u}_I^{(1)}(\pm 2\omega), \end{aligned}$$

where for convenience we introduced

$$\begin{aligned} \boldsymbol{S}(\pm 2\omega) &\equiv 2\widehat{\boldsymbol{U}}(\pm 2\omega) \cdot \left[2\widehat{\boldsymbol{U}}(\pm 2\omega) \mp i2\omega\boldsymbol{\eta} \cdot \boldsymbol{Z}(\pm 2\omega)\right]^{-1} \\ &= \widehat{\boldsymbol{U}}(\pm 2\omega) \cdot \boldsymbol{T}^{(0)}(\pm 2\omega) \cdot \widehat{\boldsymbol{U}}^{-1}(\pm 2\omega). \end{aligned} \quad (76)$$

The vectors $\boldsymbol{u}_I^{(1)}(0)$ and $\boldsymbol{u}_I^{(1)}(\pm 2\omega)$ contain each frequency component of the displacement and fluid flux in Eqs. (74a) and (74b). Therefore, using Eq. (64a), the displacements of the transmitted ($_+$) and reflected ($_-$) waves are

$$
\begin{aligned}
\boldsymbol{u}_+^{(1)}(t) &= \widehat{\boldsymbol{U}}(0)\boldsymbol{a}_+^{(1)}(0) + \widehat{\boldsymbol{U}}(2\omega)\boldsymbol{a}_+^{(1)}(2\omega)e^{-i2\omega t} + \widehat{\boldsymbol{U}}(-2\omega)\boldsymbol{a}_+^{(1)}(-2\omega)e^{i2\omega t} \\
&= \tfrac{|u_I|^2}{4}\Big(c_\eta C_2\left|\kappa_{\tau_0}\right|^2\left[\boldsymbol{I} + \mathbf{Re}\left\{\boldsymbol{S}(2\omega)e^{-2i\omega t+2i\varphi_{\tau_0}}\right\}\right]\cdot\begin{bmatrix}1\\-1\end{bmatrix} \\
&\quad + v_{g0}\phi_0 c_g^2 F_2\left|\kappa_{p_0}\right|^2\left[\boldsymbol{I} + \mathbf{Re}\left\{\boldsymbol{S}(2\omega)e^{-2i\omega t+2i\varphi_{p_0}}\right\}\right]\cdot\begin{bmatrix}0\\1\end{bmatrix}\Big),
\end{aligned}
\tag{77a}
$$

$$\boldsymbol{u}_-^{(1)}(t) = -\boldsymbol{u}_+^{(1)}(t). \tag{77b}$$

As indicated by Eqs. (72) and (77), *n*th-order displacement vectors are proportional to $(u_I)^{n+1} = (u_{3I})^{n+1}/(\varepsilon h_0)^{n+1}$ where u_{3I} is the incident wave's displacement before rescaling. Thus, the overall displacements of the transmitted ($_+$) and reflected ($_-$) waves on the fracture normalized by the amplitude of the incident wave are

$$
\begin{aligned}
&\frac{\boldsymbol{u}_{3+}(t)}{|u_{3I}|} = \frac{\boldsymbol{u}_{+}(t)}{|u_I|} = \frac{\boldsymbol{u}_{+}^{(0)}(t)+\varepsilon\boldsymbol{u}_{+}^{(1)}(t)}{|u_I|} \\
&= \mathbf{Re}\left\{\widehat{\boldsymbol{U}}(\omega)\cdot\boldsymbol{T}^{(0)}(\omega)e^{-i\omega t}\right\}\begin{bmatrix}1\\0\end{bmatrix} + \frac{1}{4}\frac{|u_{3I}|}{h_0} \\
&\times\left(c_\eta C_2|\kappa_{\tau_0}|^2\left[\boldsymbol{I}+\mathbf{Re}\left\{\boldsymbol{S}(2\omega)e^{-2i\omega t+2i\varphi_{\tau_0}}\right\}\right]\begin{bmatrix}1\\-1\end{bmatrix}\right. \\
&\left.+\phi_0 v_{g0}c_g^2F_2|\kappa_{p_0}|^2\left[\boldsymbol{I}+\mathbf{Re}\left\{\boldsymbol{S}(2\omega)e^{-2i\omega t+2i\varphi_{p_0}}\right\}\right]\cdot\begin{bmatrix}0\\1\end{bmatrix}\right),
\end{aligned}
\tag{78a}
$$

$$
\begin{aligned}
&\frac{\boldsymbol{u}_{3-}(t)}{|u_{3I}|} = \frac{\boldsymbol{u}_{-}(t)}{|u_I|} = \frac{\boldsymbol{u}_{-}^{(0)}(t)+\varepsilon\boldsymbol{u}_{-}^{(1)}(t)}{|u_I|} \\
&= \mathbf{Re}\left\{\widehat{\boldsymbol{U}}(\omega)\cdot\boldsymbol{R}^{(0)}(\omega)e^{-i\omega t}\right\}\cdot\begin{bmatrix}1\\0\end{bmatrix} - \frac{1}{4}\frac{|u_{3I}|}{h_0} \\
&\times\left(c_\eta C_2|\kappa_{\tau_0}|^2\left[\boldsymbol{I}+\mathbf{Re}\left\{\boldsymbol{S}(2\omega)e^{-2i\omega t+2i\varphi_{\tau_0}}\right\}\right]\begin{bmatrix}1\\-1\end{bmatrix}\right. \\
&\left.+\phi_0 v_{g0}c_g^2F_2|\kappa_{p_0}|^2\left[\boldsymbol{I}+\mathbf{Re}\left\{\boldsymbol{S}(2\omega)e^{-2i\omega t+2i\varphi_{p_0}}\right\}\right]\cdot\begin{bmatrix}0\\1\end{bmatrix}\right).
\end{aligned}
\tag{78b}
$$

These results indicate that the transmission and reflection coefficients of the nonlinear scattering depend on the incident wave amplitude through

$|u_{3I}|/h_0$.

Last, we pay attention to the static displacement jump, or, aperture increases. By subtracting Eq. (78b) from Eq. (78a), the static part of the jump is

$$
\frac{1}{2}\frac{|u_{3I}|}{h_0}\begin{bmatrix} c_\eta C_2|\kappa_{\tau_0}|^2 \\ -c_\eta C_2|\kappa_{\tau_0}|^2 + \phi_0 v_{g0}c_g^2F_2|\kappa_{p0}|^2\end{bmatrix}. \tag{79}
$$

Because $C_2 > 0$ (compliance increases with applied tensile stress) and $c_\eta > 0$, the first row of Eq. (79) is positive, indicating that the $n = 1$ nonlinear scattering always increases the static fracture aperture. In contrast, the behavior of fluid flux in the second row is not well constrained. However, for stiff fluid containing little gas, the second term becomes small, leaving the first term, which is identical to the displacement jump but with the opposite sign. Thus, in this case, the static effect causes influx of fluid into the fracture. This will be demonstrated by an example shown later in Figs. 8 and 9 in Sec. III B.

G. Comparison to the solution for an elastic fracture

For a system with no fluid, the fluid flux $w_{\pm}^{(n)}$, pressure $p_{\pm}^{(n)}$, and slow wave coefficients $a_{Ps\pm}^{(n)}$ in Eq. (64a) and (64b) do not exist. Thus, the coefficient matrices are reduced to scalars as

$$\widehat{\boldsymbol{U}}(\omega) \to 1,\ \boldsymbol{Z}(\omega) \to F_\sigma Z, \text{where } Z \equiv (H_U - C)s_{P_f} = (\rho H_D)^{1/2}$$

(P-wave impedance). Note that we used $s_{Pf} = (\rho/H_D)^{1/2}$ where M, $C \to 0$. The dimensionless fracture compliance matrix also is reduced as $\boldsymbol{\eta} \to F_\sigma^{-1}\eta_{D0}$. By defining a dimensionless frequency $\Omega \equiv \omega\eta_{D0}Z/2$, the parameters involved in the previous expressions are simplified as

$$\boldsymbol{T}^{(0)}(\omega) \to 1/(1 - i\Omega),\ \boldsymbol{R}^{(0)}(\omega) \to i\Omega/(1 - i\Omega),\ \kappa_{\tau_{e0}} \to 2i\Omega$$, and

$$/\eta_{D0}(1 - i\Omega),\ \kappa_{p0} \to 0$$

$$\tan\ \varphi_{\tau_{e0}} = -1/\Omega(= -1/\ \tan\ \varphi_0)$$. As a result, the displacements of the transmitted and reflected waves up to the first-order perturbation are, respectively,

$$\frac{u_{3+}(t)}{|u_{3I}|} = \frac{u_+(t)}{|u_I|} = \frac{u_+^{(0)}(t)+\varepsilon u_+^{(1)}(t)}{|u_I|}$$
$$= \frac{1}{\sqrt{1+\Omega^2}}\cos\left(-\omega t + \varphi_0\right) + C_2 \frac{|u_{3I}|}{\sigma\eta_{D0}} \frac{\Omega^2}{1+\Omega^2} \qquad (80a)$$
$$\times \left[1 + \frac{1}{\sqrt{1+4\Omega^2}}\cos\left(-2\omega t + 2\varphi_{\tau_{e0}}(\omega) + \varphi_1\right)\right],$$

$$\frac{u_{3-}(t)}{|u_{3I}|} = \frac{u_-(t)}{|u_I|} = \frac{u_-^{(0)}(t)+\varepsilon u_-^{(1)}(t)}{|u_I|}$$
$$= \frac{1}{\sqrt{1+\Omega^2}}\sin\left(-\omega t + \varphi_0\right) - C_2 \frac{|u_{3I}|}{\sigma\eta_{D0}} \frac{\Omega^2}{1+\Omega^2} \qquad (80b)$$
$$\times \left[1 + \frac{1}{\sqrt{1+4\Omega^2}}\cos\left(-2\omega t + 2\varphi_{\tau_{e0}}(\omega) + \varphi_1\right)\right],$$

Where tan $\varphi_1 \equiv 2\Omega$. Note that $1/\sigma\eta_{D0} = c_\eta/h_0$. These expressions agree with the results obtained by Biwa *et al.* (2004) and Kim *et al.* (2006) for a dry (or drained) fracture embedded in an elastic background. (Note that, however, their expressions were derived using nonlinear fracture stiffness given as a function of fracture aperture, rather than fracture compliance given as a function of the effective stress.)

III. EXAMPLES AND DISCUSSION

Using the equations derived in Sec. II F, we examine the impact of fluid in a fracture-matrix system on nonlinear seismic wave scattering. To limit the number of free parameters used in the examples, we use a set of hypothetical rock and fracture parameters in Tables I and II, considering typical sandstone properties (e.g., Berea sandstone). These properties are used to determine the poroelastic parameters of the background medium and the fracture, and frequency-dependent wave properties such as fast and slow *P* wave slownesses and the related complex coefficients $\beta_{Pf}(\omega)$ and $\beta_{Ps}(\omega)$, using the equations presented in Sec. II A. The assumed pore-tortuosity value $\alpha_\infty = 3$ is used to define the dynamic permeability model (Johnson *et al.*, 1987) used in Eq. (6).

TABLE I. Baseline background properties.

Porosity	ϕ	0.15
Pore saturation	S	1
Static permeability	k_0	10^{-12} m^2 (1 D)
Solid bulk modulus	K_s	36 GPa
Fluid bulk modulus	K_f	2.25 GPa
Frame bulk modulus	K_D	9 GPa
Frame shear modulus	G	7 GPa
Fluid viscosity	μ_f	10^{-3} Pa s (1 cP)
Solid density	ρ	2700 kg/m^3
Fluid density	ρ_f	1700 kg/m^3
Pore tortuosity	α_∞	3

TABLE II. Baseline fracture properties.[a]

Gas pressure	P_{g0}	0.1 MPa
Gas adiabatic index	γ	1.41
Fracture porosity	ϕ	0.5
Fracture gas saturation	v_{g0}	0
Fracture aperture	h_0	200 μm
Static effective stress on the fracture	$-\tau_0^*$	1 MPa
Incident fast P-wave strain[b]	ε_{Pf}^I	2.5×10^{-6}

[a]The fluid properties in the fracture are the same as the background rock.
[b]Assuming a constant strain results in incident wave amplitudes approximately inversely proportional to the wave frequency.

The fracture compliance value (drained specific normal fracture stiffness) and the nonlinear fracture compliance parameter are determined using a laboratory-measured relationship for a sandstone core containing a single, sheared fracture (Fig. 4). Note that the laboratory-measured compliances using small rock samples may be smaller than larger fractures in the field due to scale effects (e.g., Worthington and Lubbe, 2007). Also note that the sample here is subjected to the uniaxial stress condition, which may result in fracture deformation characteristics slightly different from the previously assumed uniaxial strain condition. This particular measurement resulted in a relationship between the stress and normal fracture compliance, which was best fit by a semi-logarithmic stress-deformation model (Fig. 3), which results in specific drained normal fracture compliance given by $\eta_D = -8.94 \times 10^{-6}/\tau^*$ (note that $\tau^* < 0$ for compression).

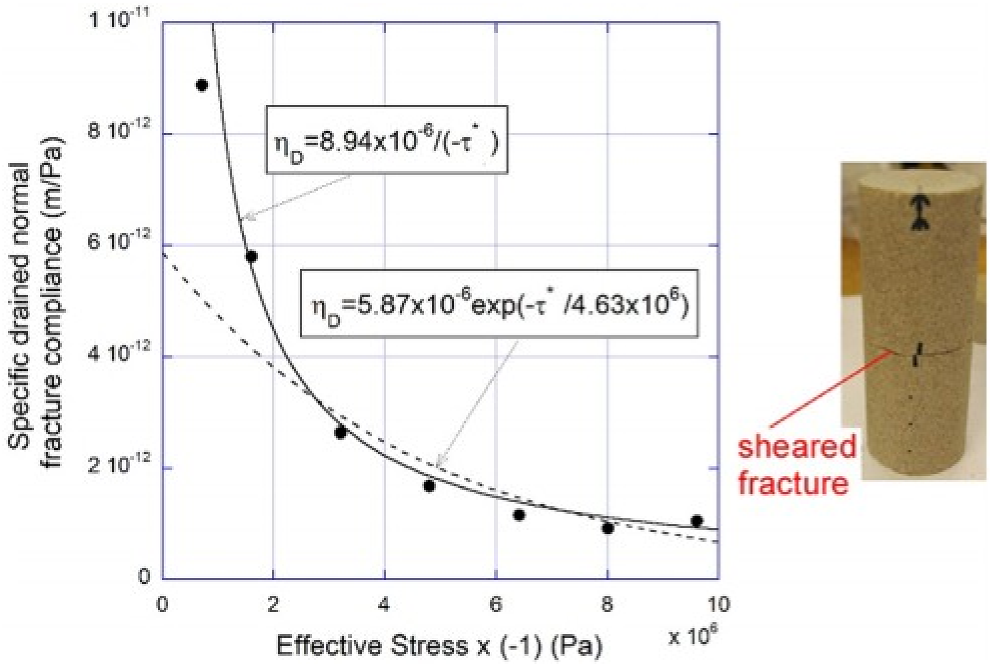

FIG. 4. (Color online) Laboratory-measured drained, normal fracture compliances as a function of the effective stress determined from resonant bar measurements at 500 Hz–1 kHz. Both best fit semi-logarithmic (top, solid curve) and exponential models (bottom, broken curve) are shown.

A. Effective stress, fracture saturation, and background permeability effects

Because slow *P* waves dissipate rapidly as the waves propagate, we examine only the scattering of fast *P* waves from an incident fast *P* wave. The transmission and reflection coefficients are computed here as the ratios of the solid displacement amplitudes, using Eqs. (72) and (77). In the following examples, the static effective stress on the fracture, fluid (water) saturation of the fracture, and the permeability of the background poroelastic medium are varied around the baseline values in Tables I and II. The assumed frequency of the incident wave is $f_c = \omega_c/2\pi = 500$ Hz, and the strain amplitude is $\pm 2.5 \times 10^{-6}$.

First, we examine the impact of static effective stress. Saturation of the fracture (by water) and the background medium's permeability are maintained at 100% and 1 D (Darcy), respectively. The effective stress is varied from 10 kPa up to 100 MPa, and the resulting transmission ($|T|$) and reflection ($|R|$) coefficients of the wave displacements are presented in Fig. 5. In this plot, the coefficients for linear scattering (frequency $\omega = \omega_c$) and first-order nonlinear scattering [$\omega = 0$ (static) and $\omega = 2\omega_c$ components] are shown separately. Note that the magnitudes of the transmission and reflection coefficients for nonlinear scattering of the same order are identical, resulting in only single curves. As a reference, the magnitudes of the perturbation parameter ε are also presented in the same scale. In this example, nonlinear scattering becomes somewhat prominent for effective stress below 1 MPa, with the $2\omega_c$ component exhibiting a peak at ≈0.5 MPa. Using somewhat higher frequencies (17–18 kHz), in the laboratory, Johnson and Jia (2005) show that a layer of very compliant porous medium (a bead pack), which can be thought of as a physical representation of our fracture, exhibits strong nonlinear acoustic behavior for strains above $\sim 1 \times 10^{-6}$ at effective stresses ~0.1 MPa. The theoretical predictions here appear to be consistent with their observation. The amplitude of the static ($\omega = 0$) component dominates the $2\omega_c$ component. Note that the value of the perturbation parameter ε becomes large with decreasing effective stress, and approaches one at ≈40 kPa. The convergence of the perturbation series is not guaranteed for such a large ε.

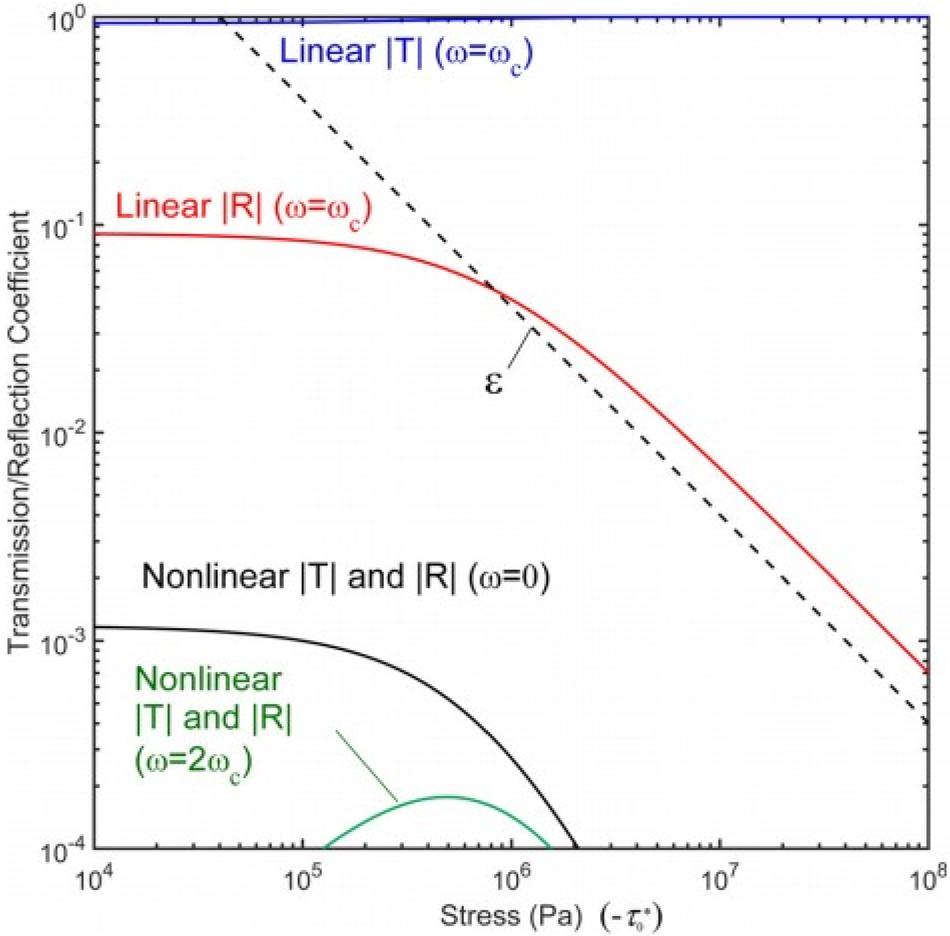

FIG. 5. (Color online) Effective stress effect on nonlinear scattering off a fracture. Background static permeability $k_0 = 1$ D, and the fracture is fully saturated by water. Incident wave frequency =500 Hz, and the strain amplitude is 2.5×10^{-6}. The nonlinear effect is relatively large for effective stress < 1 MPa.

Next, the effect of compliant gas (P_{gas} = 0.1 MPa) within a fracture is examined for an effective stress of 1 MPa and a background permeability of 1 D (Fig. 6). The effect becomes prominent once the gas saturation v_{g0} in the fracture reaches 1% where the $2\omega_c$ component exhibits a clear peak. This is attributed to the nonlinear scattering caused by the wave-induced changes of the bulk stiffness of the gas, which is shown separately by a dotted line. Because of the interference between the nonlinear scattering induced by the wave-induced changes in the fracture compliance and in the gas compliance [terms involving c_η and c_g, respectively, in Eqs. (78a) and (78b)], the $2\omega_c$ component also exhibits a sharp valley at $v_{g0} \approx 4\%$. For a fully water-saturated fracture, the transmission and reflection coefficients of the $2\omega_c$ component is about 1/10 of the drained fracture, and the static component is slightly larger.

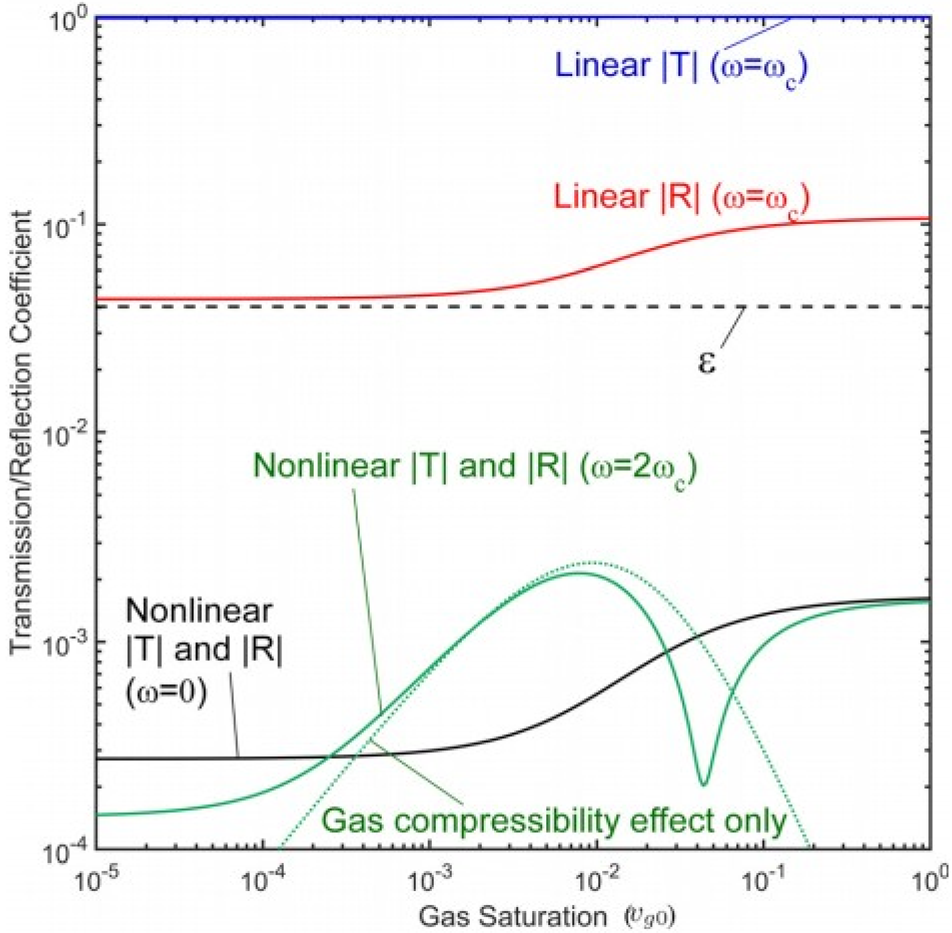

FIG. 6. (Color online) Fracture saturation effect. Static effective stress $-\tau_0^* = 1\,\mathrm{MPa}$ and the static background permeability $k_0 = 1$. The contribution of the pressure-dependent gas compliance (shown in a dotted line) results in a peak for the $2\omega_c$ scattering at about 1% gas saturation.

The last of the three examples examines the impact of the permeability of the background medium. In Fig. 7 the background permeability is varied from 1 μD up to 100 D. With increasing permeability, the enhanced wave-induced fluid flow between a fracture and the background medium relaxes the pressure within the fracture, making the fracture response more drained than undrained and resulting in larger fracture deformation. This increases both linear and nonlinear scattering as indicated by the plot. However, for the water-saturated fracture in this example, these effects are still small (linear $|R|\approx 0.07$ and nonlinear $|T|,|R|\approx 0.006$ at k_0 = 100 D).

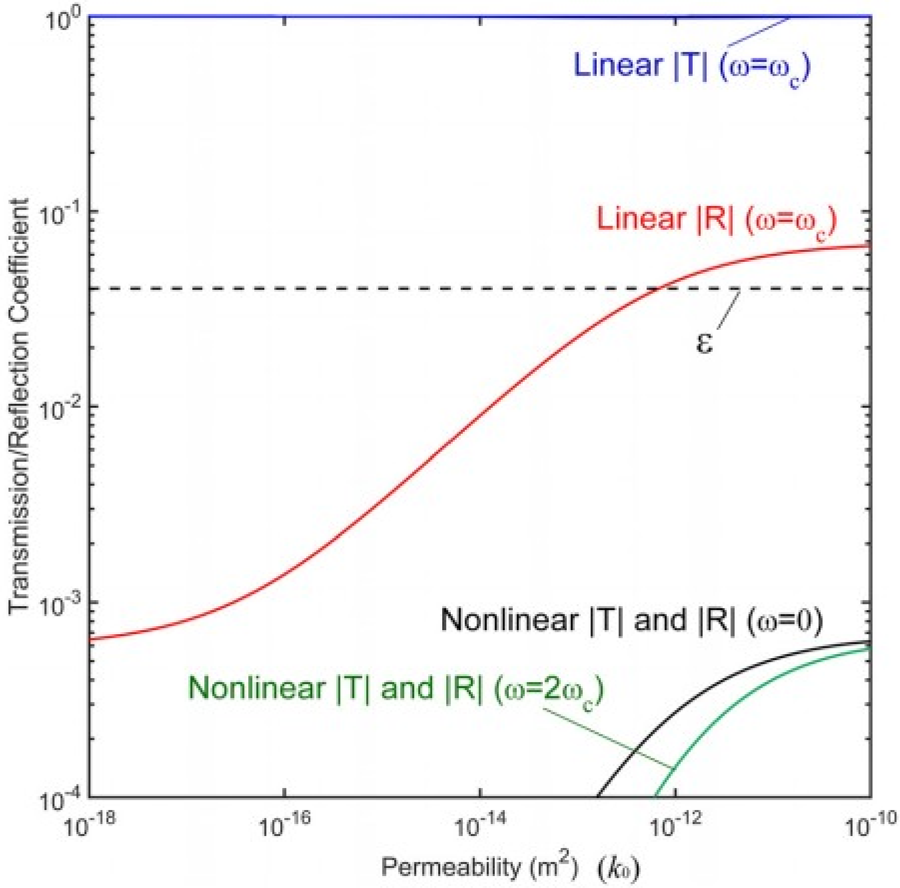

FIG. 7. (Color online) Background permeability effect. Static effective stress $-\tau_0^* = 1$ MPa and fracture saturation by water $S_F = 1$. For very high background permeability (>1 D), both linear and nonlinear scattering by the fracture become significant.

B. Transmission of transient incident waves (fast *P* waves)

In this example, we examine the impact of nonlinear scattering on transient pulses of poroelastic waves. The incident wave is a fast *P* wave with a waveform consisting of a ten-cycle (full amplitude part) cosine burst. The central frequency $f_c = \omega_c/2\pi$ is 500 Hz, wave strain is 2.5×10^{-6}, and the background and fracture parameters in Tables I and II are used. The static effective stress prior to wave arrival, fracture saturation, and the background permeability are 1 MPa, 0.5, and 1 D, respectively. Transmitted wave's solid particle displacements (Fig. 9) and pore pressures (Fig. 8) are computed for zeroth-, first-, and second-order scattering, at 0 m and 1 m away from the fracture surface. Results here include both fast and slow *P* waves in the scattered waves.

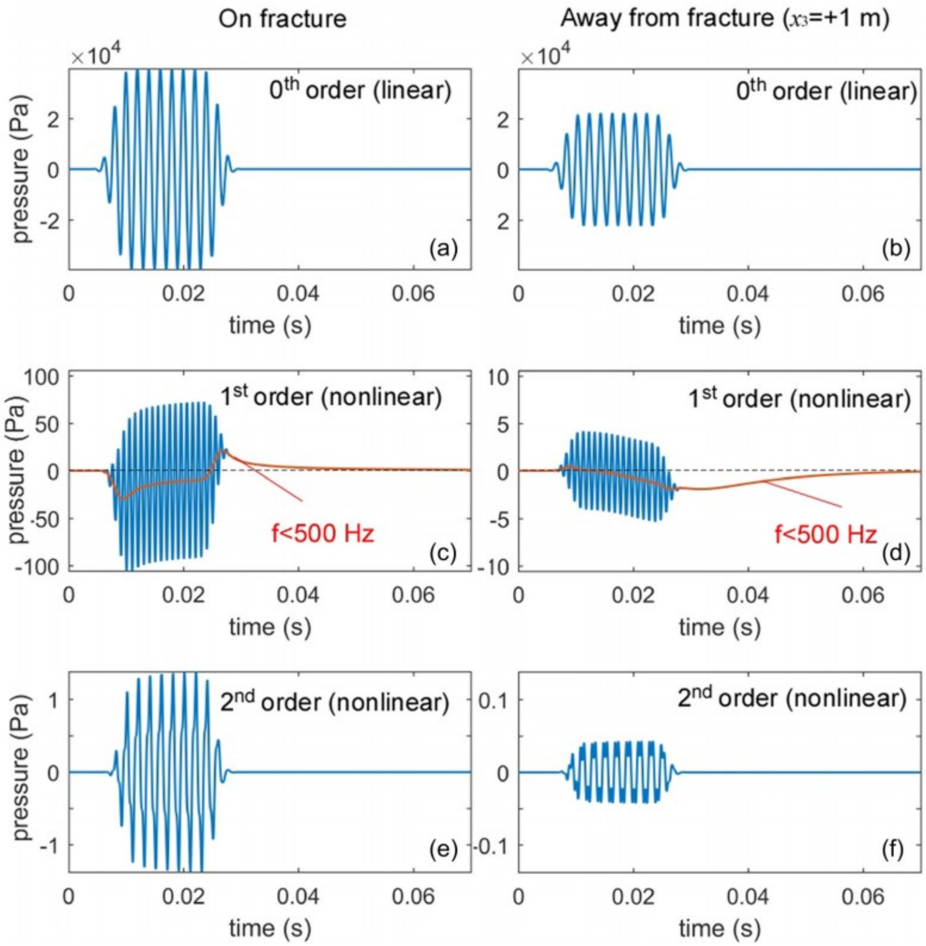

FIG. 8. (Color online) Fluid pressure responses of waves transmitted across a water-saturated fracture on ($x_3 = +0$ m) and away ($x_3 = +1$ m) from the fracture. The incident pulse is a 500 Hz cosine-wave burst. Note that the vertical scale is different between the two locations for the nonlinear scattering.

First, we examine fluid pressure responses. On (and within) the fracture, a compliant and saturated fracture produces enhanced fluid pressure changes. This results in slow *P* waves, which diffuse away from the fracture. The linear part zeroth-order scattering) of the pressure [Figs. 8(a) and 8(b)] shows a single-time-derivative form of the input displacement pulse, which decays in amplitude as it propagates away from the fracture. The first-order nonlinear part exhibits dominant 1 kHz waves, which are distorted by underlying lower-frequency waves. Low-pass (<500 Hz) filtered waveforms are superimposed in [Figs. 8(c) and 8(d)]. While the cosine burst signal is on, due to the static effect discussed in Sec. II F, negative pressure (suction) is generated by the low-frequency waves. On the fracture [Fig. 8(c)], however, the pressure starts to dissipate once the incident burst signal reaches a steady state. This is because the induced pressure diffuses away from the fracture as slow *P* waves. Near the end of the burst signal, the removal of the static effect results in positive pressure because the fluid accumulated in the fracture is trapped and has to be expelled by the reducing aperture. In contrast, away from the fracture [Fig. 8(d)], the minimum pressure is reached with some delays from the beginning of the steady state because the static-effect-induced fluid pressure changes in the fracture take some time to propagate. The reversal of the pressure signs observed on the fracture is not seen here. This is because the low-frequency slow *P* waves are strongly diffusive, and the positive pressure induced by the aperture reduction is canceled by the preceding, more dominant negative pressure in the waveform. For the current example, amplitudes of the first-order nonlinearly scattered waves ($\omega = 0$ and $2\omega_c$) are much smaller than the linearly scattered waves ($\omega = \omega_c$), and the second-order scattered waves ($\omega = \omega_c$ and $3\omega_c$) are even smaller [Figs. 8(e) and 8(f)]. This demonstrates that the related perturbation series is converging.

The accompanying solid frame displacement responses are shown in Fig. 9. Unlike the pressure response, the displacement of the linearly scattered wave does not decay rapidly as it propagates away from the fracture [Figs. 9(a) and 9(b)]. The first-order nonlinearly scattered waves exhibit prominent positive static shifts. Because the displacement on the other side of the fracture has an equal magnitude with the opposite sign, this indicates that the average fracture aperture increases while the incident wave is arriving on the fracture [Figs. 9(c) and 9(d)]. A small, slowly decaying “tail” after the incident wave disappears is caused by the closure of the fracture as the fluid accumulated by the static effect escapes and the positive pressure within the fracture reduces. Again, the amplitudes of the second-order scattered waves are much smaller than the others.

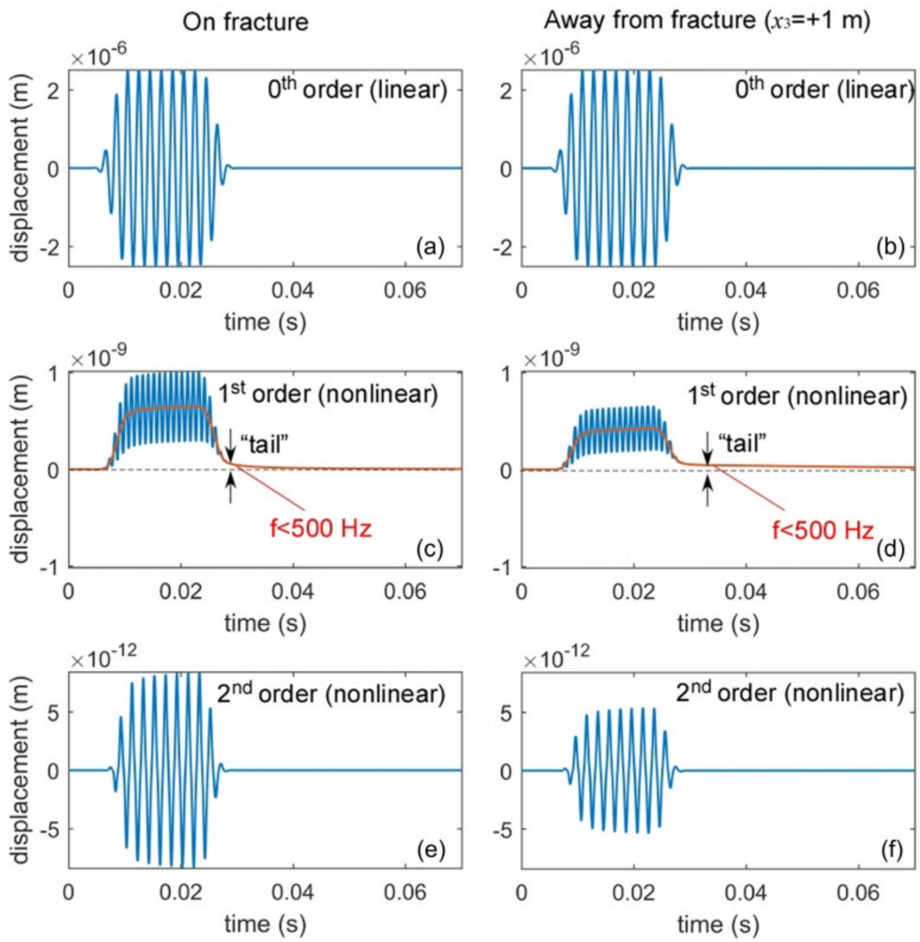

FIG. 9. (Color online) Solid frame displacement responses of transmitted waves across a water-saturated fracture on ($x_3 = +0$ m) and away ($x_3 = +1$ m) from the fracture. The incident pulse is a 500 Hz cosine-wave burst.

IV. CONCLUSIONS

In this paper, we use a perturbation method to solve the one-dimensional, nonlinear plane poroelastic wave scattering problem involving a thin, compliant, and fluid-filled interface (fracture). The behavior of the interface is modeled by a nonlinear extension of the poroelastic linear–slip interface model. With the assumption that a fracture can be modeled by a thin, compliant layer of poroelastic medium, simple expressions can be found for wave-induced finite deformation of the fracture and fluid displacement (Darcy flux) between the fracture and background medium. We found that the nonlinear fracture deformation depends only on the wave-induced effective stress while the fluid displacement depends only on the pressure.

Application of a perturbation method to the nonlinear–slip interface model results in a set of linear boundary conditions for each order of the perturbation [Eqs. (61a)–(61d)]. Except for the lowest-order linear problem, a nonlinear source term accompanies each of these conditions, which prohibits us from solving the related planewave scattering problem in the frequency domain. To solve this, the nonlinear source term in the time domain is first separated into different frequency components. Then, the linear boundary conditions are used to obtain the solutions of the scattering problem for individual frequencies, which are summed to obtain the time-domain solution. This process is applied sequentially to higher orders of perturbation, with the nonlinear source terms computed from the solutions of the lower-order scattering problems and incident wave. This method is convenient for solving problems involving linear poroelastic waves in the background medium with frequency-dependent wave propagation.

The predicted nonlinear scattering transfers wave energy from an original frequency to different frequencies. In particular, for the first-order scattering, transmitted and reflected waves of the same amplitudes but with opposite signs are produced, with both the difference frequency and sum frequency. For the first-order nonlinear scattering, the displacement amplitude of the static, difference-frequency component is generally larger than the sum-frequency component. However, a small volume of compliant gas in the fracture can significantly increase the sum-frequency component, making it larger than the static effect.

The examples revealed that, for a set of fracture and background medium properties selected in this paper, amplitudes of the nonlinearly scattered waves by a water-filled fracture are an order of magnitude or more smaller than a dry fracture, even for the relatively large strain of 2.5×10^{-6}. This is because the stiffening effect of the liquid effectively reduces wave-induced fracture aperture changes and the resulting nonlinear behavior. However, the relative magnitude of the nonlinear scattering increases for reduced static effective stress, increased background permeability, and, particularly, for inclusion of compliant gas in the fracture fluid due to the wave-induced nonlinear changes of the gas bulk modulus.

Last, the perturbation method used in this paper could produce inaccurate results when the perturbation parameter ε approaches $O(1)$. This can happen for large incident wave amplitudes (or effective stress) and for very large static fracture compliances due to small static effective stress (e.g., Fig. 5). The resulting large ε would require a longer perturbation series for more accurate solutions. For the latter, however, the dimensionless coefficients c_η, c_g, c_ℓ and the effective stress ratio $\delta\tau^*/\delta\tau^*_{\max}$, which were assumed to be $O(1)$, become small, resulting in accelerated convergence of the perturbation series. For such a case, the perturbation model presented in this paper would need to be modified. For a diverging series, the solution of the nonlinear scattering problem may need to be obtained using explicit numerical modeling such as finite-difference methods. The analytical solutions presented in this paper, however, still provide valuable physical insights into the different mechanisms by which a fracture containing fluid produces nonlinear scattering of waves.

ACKNOWLEDGMENTS

This work was supported by funding from U.S. Department of Energy (DOE) Chemical Sciences, Geosciences, and Biosciences Division under Contract No. DE-AC02-05CH11231.

REFERENCES

1.Baik, J., and Thompson, R. (1984). “ Ultrasonic scattering from imperfect interfaces,” J. Nondestr. Eval. 4, 177–196. https://doi.org/10.1007/BF00566223,

2.Bakulin, A., and Molotkov, L. (1997). “ Poroelastic medium with fractures as limiting case of stratified poroelastic medium with thin and soft biot layers,” in *67th Annual International Meeting, SEG, Expanded Abstracts*, pp. 1001–1004.

3.Bandis, S., Lumsden, A., and Barton, N. (1983). “ Fundamentals of rock joint deformation,” Int. J. Rock Mech. Min. Sci. Geomech. Abstr. 20, 249–268. https://doi.org/10.1016/0148-9062(83)90595-8,

4.Biot, M. A. (1962). “ Mechanics of deformation and acoustic propagation in porous media,” J. Appl. Phys. 33, 1482–1498. https://doi.org/10.1063/1.1728759, , ISI

5.Biwa, S., Nakajima, S., and Ohno, N. (2004). “ On the acoustic nonlinearity of solid-solid contact with pressure-dependent interface stiffness,” J. Appl. Mech. 71, 508–515. https://doi.org/10.1115/1.1767169,

6.Buck, O., Morris, W., and Richardson, J. (1978). “ Acoustic harmonic generation at unbonded interfaces and fatigue cracks,” Appl. Phys. Lett. 33(5), 371–373. https://doi.org/10.1063/1.90399, ,

7.Burridge, R., and Keller, J. B. (1981). “ Poroelasticity equations derived from microstructure,” J. Acoust. Soc. Am. 70, 1140–1146. https://doi.org/10.1121/1.386945,

8.Detournay, E. (1979). “ The interaction of deformation and hydraulic conductivity in rock fracture: An experimental and analytical study,” Master's thesis, Univ. Minnesota.

9.Donskoy, D., Sutin, A., and Ekimov, A. (2001). “ Nonlinear acoustic interaction on contact interfaces and its use for nondestructive testing,” NDT&E Int. 34, 231–238. https://doi.org/10.1016/S0963-8695(00)00063-3,

10.Goodman, R. (1976). *Methods of Geological Engineering in Discontinuous Rocks* (West Publishing, New York, NY).

11.Goodman, R., Taylor, R., and Brekke, T. (1968). “ A model for the mechanics of jointed rock,” J. Soil. Mech. Fdns. Div. 94, 637–660.

12.Greenwood, J., and Williamson, J. (1996). “ Contact of nominally flat surfaces,” Proc. R. Soc. London, Ser. A 295, 300–319. https://doi.org/10.1098/rspa.1966.0242, 13.Hirsekorn, S. (2001). “ Nonlinear transfer of ultrasound by adhesive joints—A theoretical description,” Ultrasonics 39, 57–68. https://doi.org/10.1016/S0041-624X(00)00042-1,

14.Johnson, D., Koplik, J., and Dashen, R. (1987). “ Theory of dynamic permeability and tortuosity in fluid-saturated porous media,” J. Fluid Mech. 176, 379–402. https://doi.org/10.1017/S0022112087000727,

15.Johnson, P. A., and Jia, X. (2005). “ Nonlinear dynamics, granular media and dynamic earthquake triggering,” Nature 437(7060), 871–874. https://doi.org/10.1038/nature04015,

16.Kim, J.-Y., Baltazar, A., Hu, J., and Rokhlin, S. (2006). “ Hysteretic linear and nonlinear acoustic responses from pressed interfaces,” Int. J. Solids Struct. 43, 6436–6452. https://doi.org/10.1016/j.ijsolstr.2005.11.006,

17.Korshak, B., Solodov, I., and Ballad, E. (2002). “ DC effects, sub-harmonics, stochasticity and ‘memory’ for contact acoustic non-linearity,” Ultrasonics 40, 707–713. https://doi.org/10.1016/S0041-624X(02)00241-X,

18.Lang, P., Paluszny, A., and Zimmerman, R. (2016). “ Evolution of fracture normal stiffness due to pressure dissolution and precipitation,” Int. J. Rock Mech. Min. Sci. 88, 12–22. https://doi.org/10.1016/j.ijrmms.2016.06.004,

19.Nakagawa, S., and Korneev, V. (2014). “ Effect of fracture compliance on wave propagation within a fluid-filled fracture,” J. Acoust. Soc. Am. 135, 3186–3197. https://doi.org/10.1121/1.4875333,

20.Nakagawa, S., and Schoenberg, M. (2007). “ Poroelastic modeling of seismic boundary conditions across a fracture,” J. Acoust. Soc. Am 122, 831–847. https://doi.org/10.1121/1.2747206,

21.Nayfeh, A. (2007). *Perturbation Method* (Wiley-VCH Verlag GmbH & Co. KGaA, Weinheim, Germany).

22.Pecorari, C. (2003). “ Nonlinear interaction of plane ultrasonic waves with an interface between rough surfaces in contact,” J. Acoust. Soc. Am. 113, 3065–3072. https://doi.org/10.1121/1.1570437,

23.Pride, S. (2005). “ Relationships between seismic and hydrological properties,” in *Hydrogeophysics*, edited by Y. Rubin and S. Hubbard (Springer, The Netherlands), pp. 253–290.

24.Pride, S. R., Gangi, A. F., and Morgan, F. D. (1992). “ Deriving the equations of motion for porous isotropic media,” J. Acoust. Soc. Am. 92, 3278–3290. https://doi.org/10.1121/1.404178,

25.Richardson, J. (1979). “ Harmonic generation at an unbonded interface—I. Planar interface between semi-infinite elastic media,” Int. J. Eng. Sci. 17, 73–85. https://doi.org/10.1016/0020-7225(79)90008-9, 26.Schoenberg, M. (1980). “ Elastic wave behavior across linear slip interfaces,” J. Acoust. Soc. Am. 68, 1516–1521. https://doi.org/10.1121/1.385077,

27.Van Den Abeele, K., Johnson, P., and Sutin, A. (2000). “ Nonlinear elastic wave spectroscopy (news) techniques to discern material damage, Part I: Nonlinear wave modulation spectroscopy (NWMS),” Res. Nondestruct. Eval. 12, 17–30. https://doi.org/10.1080/09349840009409646,

28.Van Den Abeele, K.-A., Carmeliet, J., Johnson, P., and Zinszner, B. (2002). “ Influence of water saturation on the nonlinear elastic mesoscopic response in earth materials and the implications to the mechanism of nonlinearity,” J. Geophys. Res.: Solid Earth 107(B6), ECV–4, https://doi.org/10.1029/2001JB000368.

29.Worthington, M., and Lubbe, R. (2007). “ The scaling of fracture compliance,” in *Fractured Reservoirs* (Geological Society of London, London), pp. 73–82.

30.Zangerl, C., Evans, K., Eberhardt, E., and Loew, S. (2008). “ Normal stiffness of fractures in granitic rock: A compilation of laboratory and in-situ experiments,” Int. J. Rock. Mech. Min. Sci. 45, 1500–1507. https://doi.org/10.1016/j.ijrmms.2008.02.001,